**Computers and Concrete**, *Vol. 31, No. 3 (2023) 223-239*
https://doi.org/10.12989/cac.2023.31.3.223


# The new flat shell element DKMGQ-CR in linear and geometric nonlinear analysis

Zuohua Li[a], Jiafei Ning[b], Qingfei Shan*, Hui Pan, Qitao Yang and Jun Teng**

*School of Civil and Environmental Engineering, Harbin Institute of Technology, Shenzhen, 518055, China*

(*Received August 2, 2022, Revised December 9, 2022, Accepted December 16, 2022*)

**Abstract.** Geometric nonlinear performance simulation and analysis of complex modern buildings and industrial products require high-performance shell elements. Balancing multiple aspects of performance in the one geometric nonlinear analysis element remains challenging. We present a new shell element, flat shell DKMGQ-CR (Co-rotational Discrete Kirchhoff-Mindlin Generalized Conforming Quadrilateral), for linear and geometric nonlinear analysis of both thick and thin shells. The DKMGQ-CR shell element was developed by combining the advantages of high-performance membrane and plate elements in a unified coordinate system and introducing the co-rotational formulation to adapt to large deformation analysis. The effectiveness of linear and geometric nonlinear analysis by DKMGQ-CR is verified through the tests of several classical numerical benchmarks. The computational results show that the proposed new element adapts to mesh distortion and effectively alleviates shear and membrane locking problems in linear and geometric nonlinear analysis. Furthermore, the DKMGQ-CR demonstrates high performance in analyzing thick and thin shells. The proposed element DKMGQ-CR is expected to provide an accurate, efficient, and convenient tool for the geometric nonlinear analysis of shells.

**Keywords:** 4-node shell finite element; co-rotation; geometric nonlinear analysis; large deformation; shear and membrane locking

## 1. Introduction

With the vigorous development of modern industry, the finite element method has been extensively used in civil engineering (Sadeghi and Nouban 2019), ocean engineering (Soeb *et al.* 2017), aerospace engineering (Träff *et al.* 2021), automobile industry (Nwuzor *et al.* 2021) and other important areas. Considering the demand for shell analysis in these industries and related research fields, the development of high-performance shell elements has important theoretical and practical significance. In particular, the simulation of structural engineering under complex conditions puts forward higher requirements on the geometric nonlinear elements (Attia *et al.* 2022, Cho *et al.* 2018, Mororó *et al.* 2020).

The flat shell has a simple structure and good applicability. Hence, researchers intend to develop various flat shell elements (Battini and Pacoste 2006, Choi and Lee 2003, Lu *et al.* 2017, Pacoste 1998). The research of flat shell elements faces some difficulties and challenges, including membrane locking, shear locking, the singularity of stiffness matrix due to lack of in-plane freedom (Ko *et al.* 2017a), and sensitivity to mesh distortion (Cen *et al.* 2019). The flat shell is composed of membrane elements and plate elements. Many approaches, including generalized conforming theory (Long and Xin 1989), Reissner-Mindlin's theory (Mindlin 1951, Reissner 1945), discrete Kirchhoff theory (Batoz *et al.* 1980, Crisfield 1984, Jeyachandrabose *et al.* 1985), and mixed interpolation of tensorial components (Bucalem and Bathe 1993, Dvorkin and Bathe 1984, Lee *et al.* 2014), have been proposed to solve these inherent difficulties. The CR (Co-rotation) method is excellent for dealing with geometric nonlinear analysis. Compared with TL (Total Lagrangian) or UL (Updated Lagrangian) method, the CR method has higher accuracy and efficiency. The normalized EICR (Element Independent Corotational Formulation) was developed in 1986 (Rankin and Brogan 1986). After decades of research (Felippa and Haugen 2005, Izzuddin 2005, Izzuddin and Liang 2016, Meek and Ristic 1997, Nour-Omid and Rankin 1991, Pacoste 1998, Rankin and Nouromid 1988) by scholars, the CR method has been widely used. Bisegna et al. presented a triangular facet shell element to analyze thin piezo-actuated structures based on the CR method (Bisegna *et al.* 2017). Deng *et al.* presented an arbitrary Lagrangian-Eulerian formulation based on the CR method to analyze planar curved viscoelastic beams (Deng *et al.* 2023). These studies demonstrate the potential of CR methods for developing geometrically nonlinear analysis elements. The existing studies have partially solved the above problems, but developing new and better high-performance elements is an ongoing pursuit. A flat shell element that comprehensively considers the problems of element

*Corresponding author, Ph.D. Student
E-mail: shanqingfei@stu.hit.edu.cn
**Corresponding author, Professor
E-mail: tengj@hit.edu.cn
[a]Professor
E-mail: lizuohua@hit.edu.cn
[b]Ph.D. Student
E-mail: ningjiafei@stu.hit.edu.cn

**Copyright © 2023 Techno-Press, Ltd.**
http://www.techno-press.org/?journal=cac&subpage=8
ISSN: 1598-8198 (Print), 1598-818X (Online)

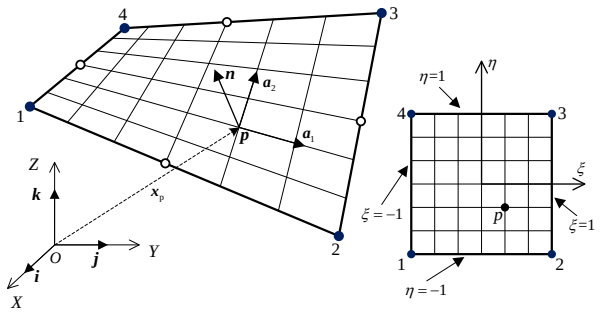


Fig. 1 Global coordinate system and natural coordinate system

conforming, thickness universality, shear locking, membrane locking, structural efficiency and geometric nonlinear is needed.

We proposed a new high-performance shell element DKMGQ-CR (Co-rotational Discrete Kirchhoff-Mindlin Generalized Conforming Quadrilateral) based on generalized conforming theory, discrete Kirchhoff plate theory, Reissner-Mindlin theory, and Co-rotational formulation. The DKMGQ-CR element thoroughly considers the conforming of elements, shear locking, membrane locking, versatility for shells of different thicknesses, capacity to resist mesh distortion, large deformation, and computational efficiency. We demonstrated the performance of the proposed shell element in linear and geometric nonlinear solutions by solving various shell problems with uniform and distorted meshes and different cases. We compared the solutions obtained by the DKMGQ-CR element with the analytical solutions or the solutions obtained by other classical elements. The results show that the DKMGQ-CR element can also obtain accurate results when the mesh distortion is relatively severe, or the element has large deformation.

## 2. Formulations of DKMGQ-CR

### *2.1 Coordinate description based on moving frame*

The following three coordinate systems are needed to describe the geometric shape of the shell element, displacement field, and global stiffness of space structure: local Cartesian coordinate system ($x$, $y$, $z$), natural coordinate system ($\xi$, $\eta$), and global Cartesian coordinate system ($X$, $Y$, $Z$).

The relative position relationship between the global coordinate system and the natural coordinate system is shown in Fig. 1 (Katili *et al.* 2015a).

The global coordinate of an arbitrary point $q$ on the element is

$$\boldsymbol{x}_q = \boldsymbol{x}_p + z\boldsymbol{n} = \sum_{i=1}^{4} N_i \boldsymbol{x}_i + z\sum_{i=1}^{4} N_i \boldsymbol{n}_i, \quad \left(-\frac{t}{2} \le z \le \frac{t}{2}\right) \tag{1}$$

where

$\boldsymbol{x}_p$ is the global coordinate of an in-plane point ($z$=0), $\boldsymbol{x}_p = [X \quad Y \quad Z]^T$

$\boldsymbol{x}_q$ is the global coordinate of an arbitrary point ($z \in [-t/2, t/2]$), $\boldsymbol{x}_q = [X_q \quad Y_q \quad Z_q]^T$

$\boldsymbol{x}_i$ is the global coordinate of node $i$ $x_i = [X_i \quad Y_i \quad Z_i]^T$,

$\boldsymbol{n}$ is the normal vector at an arbitrary point on the surface of an element

$\boldsymbol{n}_i$ is the normal vector at the point $i$ on the surface of an element, $\boldsymbol{n}_i = [n_{Xi} \quad n_{Yi} \quad n_{Zi}]^T$

$N_i$ is the shape function of a quadrilateral element, as follows

$$N_i = \frac{1}{4}(1+\xi_i\xi)(1+\eta_i\eta), \quad (i = 1,2,3,4) \tag{2}$$

The relation between the global coordinates and the natural coordinates can be obtained from $\boldsymbol{x}_p = \sum_{i=1}^{4} N_i \boldsymbol{x}_i$, as follows

$$\begin{Bmatrix} dX \\ dY \\ dZ \end{Bmatrix} = d\boldsymbol{x}_p = (\boldsymbol{x}_{p,\xi})d\xi + (\boldsymbol{x}_{p,\eta})d\eta = [\boldsymbol{a}_1 \quad \boldsymbol{a}_2]\begin{Bmatrix} d\xi \\ d\eta \end{Bmatrix} \tag{3}$$

where $a_1$ and $a_2$ can be regarded as the covariant basis, which are tangent vectors of natural coordinate axes $\xi$ and $\eta$, respectively.

$$\begin{aligned} \boldsymbol{a}_1 &= \boldsymbol{x}_{p,\xi} = \sum_{i=1}^{4} N_{i,\xi}\boldsymbol{x}_i \\ \boldsymbol{a}_2 &= \boldsymbol{x}_{p,\eta} = \sum_{i=1}^{4} N_{i,\eta}\boldsymbol{x}_i \end{aligned} \tag{4}$$

where $N_{i,\xi}$ and $N_{i,\eta}$ are the first partial derivatives of the shape function.

The point-wise local coordinate basis is $\boldsymbol{F}_0 = [\boldsymbol{a}_1 \quad \boldsymbol{a}_2 \quad \boldsymbol{n}]$, where $\boldsymbol{n}$ is the unit vector of the $z$-axis

$$\boldsymbol{n} = \frac{\boldsymbol{a}_1 \times \boldsymbol{a}_2}{|\boldsymbol{a}_1 \times \boldsymbol{a}_2|} \tag{5}$$

The metric tensor of a plane in the element is

$$\boldsymbol{a} = \begin{bmatrix} a_{11} & a_{12} \\ a_{21} & a_{22} \end{bmatrix} = \begin{bmatrix} \boldsymbol{a}_1 \cdot \boldsymbol{a}_1 & \boldsymbol{a}_1 \cdot \boldsymbol{a}_2 \\ \boldsymbol{a}_2 \cdot \boldsymbol{a}_1 & \boldsymbol{a}_2 \cdot \boldsymbol{a}_2 \end{bmatrix} \tag{6}$$

The vector of the elemental area of the surface is

$$d\boldsymbol{A} = \boldsymbol{a}_1 d\xi \times \boldsymbol{a}_2 d\eta = |\boldsymbol{a}_1 \times \boldsymbol{a}_2| d\xi d\eta \cdot \boldsymbol{n} = \sqrt{|\boldsymbol{a}|} \cdot d\xi d\eta \cdot \boldsymbol{n} = dA \cdot \boldsymbol{n} \tag{7}$$

where the elemental area is expressed as

$$dA = \sqrt{|\boldsymbol{a}|} \cdot d\xi d\eta \tag{8}$$

The contravariant basis $a^1$ and $a^2$ are introduced to simplify the formulations, define $[\boldsymbol{a}^1 \quad \boldsymbol{a}^2 \quad \boldsymbol{n}]^T = \boldsymbol{F_0}^{-1}$, then

$$[\boldsymbol{a}^1 \quad \boldsymbol{a}^2 \quad \boldsymbol{n}]^T [\boldsymbol{a}_1 \quad \boldsymbol{a}_2 \quad \boldsymbol{n}] = \boldsymbol{I} \tag{9}$$

Then the two vectors $a^1$ and $a^2$ are expressed as

$$\begin{aligned} \boldsymbol{a}^1 &= \frac{1}{|\boldsymbol{a}|}(a_{22}\boldsymbol{a}_1 - a_{21}\boldsymbol{a}_2) \\ \boldsymbol{a}^2 &= \frac{1}{|\boldsymbol{a}|}(-a_{12}\boldsymbol{a}_1 + a_{11}\boldsymbol{a}_2) \end{aligned} \tag{10}$$

It can be inferred from Eqs. (3), (9) and (10) that

$$\begin{Bmatrix} d\xi \\ d\eta \end{Bmatrix} = [\boldsymbol{a}^1 \quad \boldsymbol{a}^2]^T \begin{Bmatrix} dX \\ dY \\ dZ \end{Bmatrix} \tag{11}$$

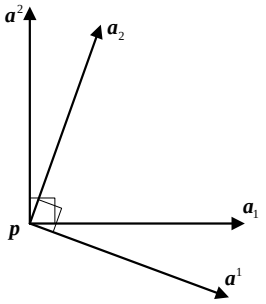


Fig. 2 Covariant and contravariant basis

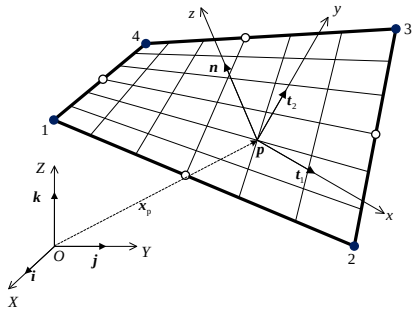


Fig. 3 Global coordinate system and local Cartesian coordinate system

Based on Eqs. (3) and (11), $[a_1 \quad a_2]$ are covariant basis and $[a^1 \quad a^2]^T$ are contravariant basis between global and natural coordinate systems (Katili *et al.* 2015a), which are shown in Fig. 2.

The relationship between the global coordinate system and the local Cartesian coordinate system is shown in Fig. 3 (Katili *et al.* 2015a).

Also, the relationship of two coordinate systems in Fig. 3 can be expressed as

$$\begin{Bmatrix} dX \\ dY \\ dZ \end{Bmatrix} = \boldsymbol{Q} \begin{Bmatrix} dx \\ dy \\ dz \end{Bmatrix} \tag{12}$$

where

$$\boldsymbol{Q} = [\boldsymbol{t}_1 \quad \boldsymbol{t}_2 \quad \boldsymbol{n}] \tag{13}$$

where

$$\begin{gathered} \boldsymbol{t}_1 = \frac{\boldsymbol{n}\times\boldsymbol{k}}{|\boldsymbol{n}\times\boldsymbol{k}|}, \text{ if } \boldsymbol{n} \neq \pm\boldsymbol{k} \\ \boldsymbol{t}_1 = \boldsymbol{i} \quad , \text{if } \boldsymbol{n} = \pm\boldsymbol{k} \\ \boldsymbol{t}_2 = \frac{\boldsymbol{n}\times\boldsymbol{t}_1}{|\boldsymbol{n}\times\boldsymbol{t}_1|} \end{gathered} \tag{14}$$

The nodes of the local Cartesian coordinate system and the natural coordinate system are one-to-one correspondence. The four nodes of the element are

numbered in the order of counterclockwise direction, as shown in Fig. 4.

Combine Eqs. (11)-(12), we can derive that the conversion relation between the natural coordinate and the local Cartesian coordinate system is

$$\begin{Bmatrix} d\xi \\ d\eta \end{Bmatrix} = \boldsymbol{C}^0 \begin{Bmatrix} dx \\ dy \end{Bmatrix} \tag{15}$$

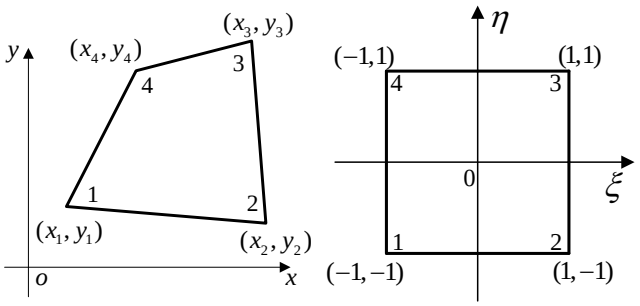


(a) Local Cartesian coordinate system (b) Natural coordinate system

Fig. 4 (a) Local Cartesian coordinate system and (b) Natural coordinate system (for 4-node element)

where

$$\boldsymbol{C}^0 = \begin{bmatrix} C_{11}^0 & C_{12}^0 \\ C_{21}^0 & C_{22}^0 \end{bmatrix} = \begin{bmatrix} \boldsymbol{a}^1\boldsymbol{t}_1 & \boldsymbol{a}^1\boldsymbol{t}_2 \\ \boldsymbol{a}^2\boldsymbol{t}_1 & \boldsymbol{a}^2\boldsymbol{t}_2 \end{bmatrix} \tag{16}$$

We can deduce the relationship between the first order partial derivative $N_{\forall,(x,y)}$ of arbitrary shape function to the local coordinate axis and the first order partial derivative $N_{\forall,(\xi,\eta)}$ of arbitrary shape function to the natural coordinate axis from the relationship between natural coordinates and local coordinates, as follows

$$\begin{Bmatrix} \frac{\partial N_\forall}{\partial x} \\ \frac{\partial N_\forall}{\partial y} \end{Bmatrix} = (\boldsymbol{C}^0)^T \begin{Bmatrix} \frac{\partial N_\forall}{\partial \xi} \\ \frac{\partial N_\forall}{\partial \eta} \end{Bmatrix} \tag{17}$$

### *2.2 Linear formulations of DKMGQ-CR*

Some shell elements have only five DOFs (degrees of freedom) per node, missing one in-plane rotation DOF, while the most popular spatial beam elements have six DOFs per node. Additional modeling and computational work are needed when shell elements (with five DOFs per node) and beam elements (with six DOFs per node) are modelled together (Lu *et al.* 2017). Six DOFs per node for the new shell element are necessary to avoid additional work and improve accuracy. Generally, a flat shell element consists of a membrane element and a plate element, as shown in Fig. 5. The membrane has three DOFs ($u$, $v$ and $\theta_z$) per node, and the plate also has three DOFs ($w$, $\theta_x$ and $\theta_y$) per node.

There are six DOFs at each node of the shell as follows

$$\boldsymbol{\delta}_i^e = [u_i \quad v_i \quad w_i \quad \theta_{xi} \quad \theta_{yi} \quad \theta_{zi}]^T, (i = 1,2,3,4) \tag{18}$$

For quadrilateral shell elements, the nodal displacement vector is

$$\boldsymbol{\delta}^e = [\boldsymbol{\delta}_1^s \quad \boldsymbol{\delta}_2^s \quad \boldsymbol{\delta}_3^s \quad \boldsymbol{\delta}_4^s]^T \tag{19}$$

#### *2.2.1 Formulations of the membrane and plate element*

The properties of the shell element are highly dependent on the properties of the membrane and plate element that comprise it.

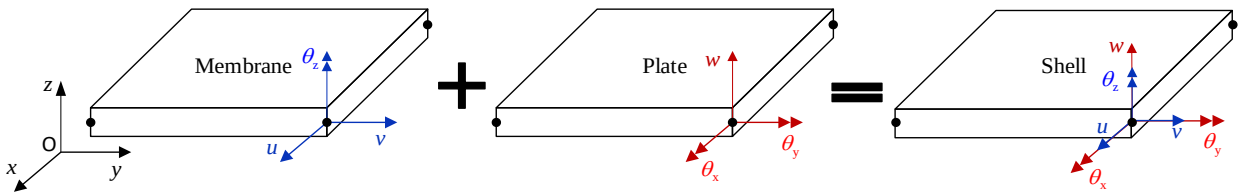


Fig. 5 Assembly of the flat shell element

GQ12 (Xu and Long 1993) is a 4-node membrane element with three DOFs per node. The displacement of each node is

$$\boldsymbol{\delta}_{mi} = [u_i \quad v_i \quad \theta_{zi}]^T, (i = 1,2,3,4) \tag{20}$$

where $u_i$ and $v_i$ are the translational displacement, $\theta_{zi}$ is the rotational displacement in the additional plane of the node.

Displacement vector of the element node can be written as

$$\boldsymbol{\delta}_m = [\boldsymbol{\delta}_{m1} \quad \boldsymbol{\delta}_{m2} \quad \boldsymbol{\delta}_{m3} \quad \boldsymbol{\delta}_{m4}]^T \tag{21}$$

The displacement field $\omega$ in the local coordinate system consists of a bilinear coordinated displacement field and an additional rigid body rotation displacement field.

The displacement field of GQ12 is

$$\boldsymbol{\omega} = \boldsymbol{\omega}_0 + \boldsymbol{\omega}_\theta \tag{22}$$

where

$$\begin{aligned} \boldsymbol{\omega}_0 &= \begin{Bmatrix} u_0 \\ v_0 \end{Bmatrix} = \sum_{i=1}^{4} \begin{bmatrix} N_i & 0 \\ 0 & N_i \end{bmatrix} \begin{Bmatrix} u_i \\ v_i \end{Bmatrix} \\ \boldsymbol{\omega}_\theta &= \begin{Bmatrix} u_\theta \\ v_\theta \end{Bmatrix} = \sum_{i=1}^{4} \begin{Bmatrix} N_{u\theta i} \\ N_{v\theta i} \end{Bmatrix} \theta_{zi} \end{aligned} \tag{23}$$

Then the formula of the displacement field can be obtained as follows

$$\begin{aligned} \boldsymbol{\omega} = \begin{Bmatrix} u \\ v \end{Bmatrix} = \begin{Bmatrix} u_0 + u_\theta \\ v_0 + v_\theta \end{Bmatrix} = \boldsymbol{N}^m \boldsymbol{\delta}^m = \\ \sum_{i=1}^{4} \begin{bmatrix} N_i & 0 & N_{u\theta i} \\ 0 & N_i & N_{v\theta i} \end{bmatrix} \begin{Bmatrix} u_i \\ v_i \\ \theta_{zi} \end{Bmatrix} = \sum_{i=1}^{4} \boldsymbol{N}^i \boldsymbol{\delta}_i^m \end{aligned} \tag{24}$$

where $N_i$, $N_{u\theta i}$, and $N_{v\theta i}$ can be written in detail as follows (Xu and Long 1993)

$$\begin{cases} N_i = \frac{1}{4}(1+\xi_i\xi)(1+\eta_i\eta) \\ N_{u\theta i} = \frac{1}{8}[\xi_i(1-\xi^2)(b_1+b_3\eta_i)(1+\eta_i\eta) + \\ \quad \eta_i(1-\eta^2)(b_2+b_3\xi_i)(1+\xi_i\xi)] \\ N_{v\theta i} = -\frac{1}{8}[\xi_i(1-\xi^2)(a_1+a_3\eta_i)(1+\eta_i\eta) \\ \quad +\eta_i(1-\eta^2)(a_2+a_3\xi_i)(1+\xi_i\xi)] \end{cases} \tag{25}$$

where $a_1$, $a_2$, $a_3$, $b_1$, $b_2$, $b_3$ are

$$\begin{cases} a_1 = \frac{1}{4}\sum_{i=1}^{4}\xi_i x_i, a_2 = \frac{1}{4}\sum_{i=1}^{4}\eta_i x_i, a_3 = \frac{1}{4}\sum_{i=1}^{4}\xi_i\eta_i x_i, \\ b_1 = \frac{1}{4}\sum_{i=1}^{4}\xi_i y_i, b_2 = \frac{1}{4}\sum_{i=1}^{4}\eta_i y_i, b_3 = \frac{1}{4}\sum_{i=1}^{4}\xi_i\eta_i y_i, \end{cases} \tag{26}$$

The strain matrix of membrane element in the local coordinate system is

$$\varepsilon_m = \begin{Bmatrix} \varepsilon_x \\ \varepsilon_y \\ \gamma_{xy} \end{Bmatrix} = \begin{Bmatrix} \frac{\partial u}{\partial x} \\ \frac{\partial v}{\partial y} \\ \frac{\partial u}{\partial y} + \frac{\partial v}{\partial x} \end{Bmatrix} = \boldsymbol{B}_m \boldsymbol{\delta}_m \tag{27}$$

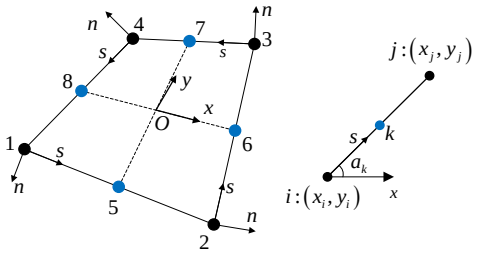


Fig. 6 8-node plate element

where

$$\boldsymbol{B}_m = [\boldsymbol{B}_{m1} \quad \boldsymbol{B}_{m2} \quad \boldsymbol{B}_{m3} \quad \boldsymbol{B}_{m4}] \tag{28}$$

where $\boldsymbol{B}_{mi}$ ($i$=1, 2, 3, 4) is

$$\boldsymbol{B}_{mi} = \begin{bmatrix} \frac{\partial N_i}{\partial x} & 0 & \frac{\partial N_{u\theta i}}{\partial x} \\ 0 & \frac{\partial N_i}{\partial y} & \frac{\partial N_{v\theta i}}{\partial y} \\ \frac{\partial N_i}{\partial y} & \frac{\partial N_i}{\partial x} & \frac{\partial N_{u\theta i}}{\partial y} + \frac{\partial N_{v\theta i}}{\partial x} \end{bmatrix} \tag{29}$$

The stiffness matrix of membrane element in the local coordinate system is

$$\boldsymbol{K}_m = \int_A \boldsymbol{B}_m^T \boldsymbol{H}_m \boldsymbol{B}_m dA = \int_{-1}^{1}\int_{-1}^{1} \boldsymbol{B}_m^T \boldsymbol{H}_m \boldsymbol{B}_m \sqrt{|\boldsymbol{a}|} \cdot d\xi d\eta \tag{30}$$

where

$$\boldsymbol{H}_m = D_m \begin{bmatrix} 1 & \mu & 0 \\ \mu & 1 & 0 \\ 0 & 0 & \frac{1-\mu}{2} \end{bmatrix}, \quad D_m = \frac{Et}{1-\mu^2} \tag{31}$$

$E$ is elasticity modulus,
$\mu$ is Poisson's ratio,
$t$ is thickness.

DKMQ (Katili 1993, Katili *et al.* 2015b, 2015a, Wong *et al.* 2017) is a 4-node quadrilateral plate element based on the Reissner-Mindlin theory that reduces shear locking. The right-handed rule determines the positive direction of the rotation angle. The three DOFs of the joint are deflection $w$, rotation around $x$-axis $\theta_x$=$\beta_y$, and rotation around $y$-axis $\theta_y$=-$\beta_x$.

The DKMQ plate element adds a midpoint to each edge of the element and condenses the DOFs of the four midpoints. The 8-node plate is shown in Fig. 6.

Define that

$$\begin{aligned} x_{ji} &= x_j - x_i \\ y_{ji} &= y_j - y_i \\ C_k &= cosa_k = x_{ji}/L_k \\ S_k &= sina_k = y_{ji}/L_k \\ {L_k}^2 &= {x_{ji}}^2 + {y_{ji}}^2 \end{aligned} \tag{32}$$

The displacement vector of every node includes 3 DOFs, which can be shown as

$$\boldsymbol{\delta}_{pi} = [w_i \quad \theta_{xi} \quad \theta_{yi}]^T, (i = 1,2,3,4) \tag{33}$$

The displacement vector of the plate element is

$$\boldsymbol{\delta}_p = [\boldsymbol{\delta}_{p1} \quad \boldsymbol{\delta}_{p2} \quad \boldsymbol{\delta}_{p3} \quad \boldsymbol{\delta}_{p4}]^T \tag{34}$$

DOFs of the normal rotation angle of the midpoints can be expressed as

$$\Delta\boldsymbol{\beta}_n = [\Delta\beta_{s5} \quad \Delta\beta_{s6} \quad \Delta\beta_{s7} \quad \Delta\beta_{s8}]^T \tag{35}$$

The cross-section rotation field is composed of a rigid body constant curvature field and a high-order interpolation function since the deflection of the plate is a bilinear field, as follows

$$\begin{cases} \beta_x = -\sum_{i=1}^{4} N_i\theta_{yi} - \sum_{k=5}^{8} N_k C_k \Delta\beta_{sk} \\ \beta_y = \sum_{i=1}^{4} N_i\theta_{xi} - \sum_{k=5}^{8} N_k S_k \Delta\beta_{sk} \end{cases} \tag{36}$$

where the shape function is

$$N_i = \begin{cases} \frac{1}{4}(1+\xi_i\xi)(1+\eta_i\eta), & (i = 1,2,3,4) \\ \frac{1}{2}(1-\xi^2)(1+\eta_i\eta), & (i = 5,7) \\ \frac{1}{2}(1-\eta^2)(1+\xi_i\xi), & (i = 6,8) \end{cases} \tag{37}$$

Strain matrices of bending and shearing, respectively, are

$$\begin{cases} \boldsymbol{B}_b = \boldsymbol{B}_{b\beta} + \boldsymbol{B}_{b\Delta\beta}\boldsymbol{A}_n \\ \boldsymbol{B}_s = \boldsymbol{B}_{s\Delta\beta}\boldsymbol{A}_n \end{cases} \tag{38}$$

where $B_{b\beta}$ can be expressed as

$$\boldsymbol{B}_{b\beta} = [\boldsymbol{B}_{b\beta1}\boldsymbol{B}_{b\beta2}\boldsymbol{B}_{b\beta3}\boldsymbol{B}_{b\beta4}]_{(3\times12)} \tag{39}$$

$$\boldsymbol{B}_{b\beta i} = \begin{bmatrix} 0 & 0 & \frac{\partial N_i}{\partial x} \\ 0 & -\frac{\partial N_i}{\partial y} & 0 \\ 0 & -\frac{\partial N_i}{\partial x} & \frac{\partial N_i}{\partial y} \end{bmatrix}, (i = 1,2,3,4) \tag{40}$$

$$\begin{cases} \frac{\partial N_i}{\partial x} = \frac{\partial N_i}{\partial \xi}C_{11}^0 + \frac{\partial N_i}{\partial \eta}C_{21}^0 \\ \frac{\partial N_i}{\partial y} = \frac{\partial N_i}{\partial \xi}C_{12}^0 + \frac{\partial N_i}{\partial \eta}C_{22}^0 \end{cases} \tag{41}$$

$\boldsymbol{B}_{b\Delta\beta}$ can be expressed as

$$\boldsymbol{B}_{b\Delta\beta} = [\boldsymbol{B}_{b\Delta\beta1}\boldsymbol{B}_{b\Delta\beta2}\boldsymbol{B}_{b\Delta\beta3}\boldsymbol{B}_{b\Delta\beta4}]_{(3\times4)} \tag{42}$$

where the components of $\boldsymbol{B}_{b\Delta\beta}$ are

$$\boldsymbol{B}_{b\Delta\beta i} = \begin{Bmatrix} \frac{\partial N_k}{\partial x}C_k \\ \frac{\partial N_k}{\partial y}S_k \\ \frac{\partial N_k}{\partial y}C_k + \frac{\partial N_k}{\partial x}S_k \end{Bmatrix}, (i,k) \in \{(1,5),(2,6),(3,7),(4,8)\} \tag{43}$$

where

$$\begin{cases} \frac{\partial N_k}{\partial x} = \frac{\partial N_k}{\partial \xi}C_{11}^0 + \frac{\partial N_k}{\partial \eta}C_{21}^0 \\ \frac{\partial N_k}{\partial y} = \frac{\partial N_k}{\partial \xi}C_{12}^0 + \frac{\partial N_k}{\partial \eta}C_{22}^0 \end{cases} \tag{44}$$

Moreover, the strain matrix of shearing $\boldsymbol{B}_{s\Delta\beta}$ can be expressed as

$$B_{s\Delta\beta} = \frac{1}{6}\begin{bmatrix} -C_{11}^0(1-\eta)L_5\phi_5 & -C_{21}^0(1+\xi)L_6\phi_6 & C_{11}^0(1+\eta)L_7\phi_7 & C_{21}^0(1-\xi)L_8\phi_8 \\ -C_{12}^0(1-\eta)L_5\phi_5 & -C_{22}^0(1+\xi)L_6\phi_6 & C_{12}^0(1+\eta)L_7\phi_7 & C_{22}^0(1-\xi)L_8\phi_8 \end{bmatrix} \tag{45}$$

Matrix $\boldsymbol{A}_n$ is a transformation matrix between $\boldsymbol{\delta}_p$ and $\Delta\boldsymbol{\beta}_n$.

$$\boldsymbol{A}_n\boldsymbol{\delta}_p = \Delta\boldsymbol{\beta}_n \tag{46}$$

Then

$$\boldsymbol{A}_n = \boldsymbol{A}_\Delta^{-1}\boldsymbol{A}_w \tag{47}$$

where

$$\boldsymbol{A}_\Delta = \frac{2}{3}\begin{bmatrix} L_5(1+\phi_5) & 0 & 0 & 0 \\ 0 & L_6(1+\phi_6) & 0 & 0 \\ 0 & 0 & L_7(1+\phi_7) & 0 \\ 0 & 0 & 0 & L_8(1+\phi_8) \end{bmatrix} \tag{48}$$

$$\boldsymbol{A}_w = \begin{bmatrix} 1 & \frac{y_{21}}{2} & \frac{-x_{21}}{2} & -1 & \frac{y_{21}}{2} & \frac{-x_{21}}{2} & 0 & 0 & 0 & 0 & 0 & 0 \\ 0 & 0 & 0 & 1 & \frac{y_{32}}{2} & \frac{-x_{32}}{2} & -1 & \frac{y_{32}}{2} & \frac{-x_{32}}{2} & 0 & 0 & 0 \\ 0 & 0 & 0 & 0 & 0 & 0 & 1 & \frac{y_{43}}{2} & \frac{-x_{43}}{2} & -1 & \frac{y_{43}}{2} & \frac{-x_{43}}{2} \\ -1 & \frac{y_{14}}{2} & \frac{-x_{14}}{2} & 0 & 0 & 0 & 0 & 0 & 0 & 1 & \frac{y_{14}}{2} & \frac{-x_{14}}{2} \end{bmatrix} \tag{49}$$

The shear influence coefficient $\phi_k$ in Eq. (48) is

$$\phi_k = \frac{2}{k(1-\mu)}\left(\frac{t^2}{L_k^2}\right), \left(k = \frac{5}{6}\right) \tag{50}$$

The relationship between bending moment and shear curvature is

$$\begin{Bmatrix} M_x \\ M_y \\ M_{xy} \end{Bmatrix} = \boldsymbol{H}_b\boldsymbol{\chi}_b, \quad \boldsymbol{H}_b = D_b\begin{bmatrix} 1 & \mu & 0 \\ \mu & 1 & 0 \\ 0 & 0 & \frac{1-\mu}{2} \end{bmatrix}, \quad D_b = \frac{Et^3}{12(1-\mu^2)} \tag{51}$$

$$\begin{Bmatrix} T_x \\ T_y \end{Bmatrix} = \boldsymbol{H}_s\boldsymbol{\gamma}, \quad \boldsymbol{H}_s = D_s\begin{bmatrix} 1 & 0 \\ 0 & 1 \end{bmatrix}, \quad D_s = \frac{Ekt}{2(1+\mu)} \tag{52}$$

where

$E$ is the elastic modulus,
$\mu$ is the Poisson ratio,
$t$ is the thickness of the element,
$k$ is the shear coefficient.

Then we get the bending stiffness formula as follows

$$\boldsymbol{K}_b = \int_A \boldsymbol{B}_b^T\boldsymbol{H}_b\boldsymbol{B}_b dA = \int_{-1}^{1}\int_{-1}^{1} \boldsymbol{B}_b^T\boldsymbol{H}_b\boldsymbol{B}_b\sqrt{|\boldsymbol{a}|}\cdot d\xi d\eta \tag{53}$$

The shear stiffness formula is

$$\boldsymbol{K}_s = \int_A \boldsymbol{B}_s^T\boldsymbol{H}_s\boldsymbol{B}_s dA = \int_{-1}^{1}\int_{-1}^{1} \boldsymbol{B}_s^T\boldsymbol{H}_s\boldsymbol{B}_s\sqrt{|\boldsymbol{a}|}\cdot d\xi d\eta \tag{54}$$

The total stiffness matrix in a local coordinate system of the plate is

$$\boldsymbol{K}_p = \boldsymbol{K}_b + \boldsymbol{K}_s \tag{55}$$

### *2.2.2 Linear stiffness matrix formulation of DKMGQ-CR*

The stiffness matrix of shell element DKMGQ-CR is a 24×24 symmetry matrix composed of $\boldsymbol{K}_m$ and $\boldsymbol{K}_p$ according

to the position index of their respective DOFs. For one DOF of the element DKMGQ-CR, the linear stiffness matrix is composed as follows

$$\boldsymbol{K}_{ij}^{\mathrm{e}}=\begin{array}{c}\begin{matrix}u_i & v_i & \theta_{xi} & \theta_{yi} & \theta_{zi} & w_i\end{matrix}\\ \left[\begin{array}{ccccc|c} & & 0 & 0 & 0 & \\ & \boldsymbol{K}_{ij}^{\mathrm{m}} & 0 & 0 & 0 & \boldsymbol{K}_{ij}^{\mathrm{m}} \\ \hline 0 & 0 & & & & 0 \\ 0 & 0 & & \boldsymbol{K}_{ij}^{\mathrm{p}} & & 0 \\ 0 & 0 & & & & 0 \\ \hline & \boldsymbol{K}_{ij}^{\mathrm{m}} & 0 & 0 & 0 & \boldsymbol{K}_{ij}^{\mathrm{m}} \end{array}\right]\end{array}\begin{matrix}u_i\\ v_i\\ \theta_{xi}\\ \theta_{yi}\\ \theta_{zi}\\ w_i\end{matrix} \tag{56}$$

where

$\boldsymbol{K}_{ij}^{m}$ is the corresponding elements of $\boldsymbol{K}_m$

$\boldsymbol{K}_{ij}^{p}$ is the corresponding elements of $\boldsymbol{K}_p$

Coordinate transformations are necessary to place all elements in the global coordinate system. The cosine of the angle between the local coordinate axis and the global coordinate axis can be expressed by a matrix $\boldsymbol{\lambda}$

$$\boldsymbol{\lambda}=[\boldsymbol{t}_1 \quad \boldsymbol{t}_2 \quad \boldsymbol{n}]^T \tag{57}$$

The element stiffness matrix in global coordinates can be expressed as

$$\boldsymbol{K}=\boldsymbol{T}^T\boldsymbol{K}^e\boldsymbol{T} \tag{58}$$

where $\boldsymbol{T}$ is the transfer matrix between the local Cartesian and global coordinates, as follows

$$\boldsymbol{T}=\begin{bmatrix}\boldsymbol{L} & \boldsymbol{0} & \boldsymbol{0} & \boldsymbol{0}\\ \boldsymbol{0} & \boldsymbol{L} & \boldsymbol{0} & \boldsymbol{0}\\ \boldsymbol{0} & \boldsymbol{0} & \boldsymbol{L} & \boldsymbol{0}\\ \boldsymbol{0} & \boldsymbol{0} & \boldsymbol{0} & \boldsymbol{L}\end{bmatrix},\boldsymbol{L}=\begin{bmatrix}\boldsymbol{\lambda} & \boldsymbol{0}\\ \boldsymbol{0} & \boldsymbol{\lambda}\end{bmatrix} \tag{59}$$

#### 2.2.3 Equivalent nodal load of uniform surface load

The nodal load vector in the global coordinate system of the shell element is

$$\boldsymbol{F}^e=[\boldsymbol{F}_1 \quad \boldsymbol{F}_2 \quad \boldsymbol{F}_3 \quad \boldsymbol{F}_4]^T \tag{60}$$

The load vector for each node is

$$\boldsymbol{F}_i=[F_{xi} \quad F_{yi} \quad M_{zi} \quad M_{\theta xi} \quad M_{\theta yi} \quad M_{\theta zi}],\ (i=1,2,3,4) \tag{61}$$

Then the equivalent nodal load of a uniform surface load of shell element DKMGQ-CR in the global coordinate system is

$$\boldsymbol{F}_i^T=\int_A N_i\begin{Bmatrix}q_x\\ q_y\\ q_z\\ 0\\ 0\\ 0\end{Bmatrix}dA=\begin{Bmatrix}q_x\\ q_y\\ q_z\\ 0\\ 0\\ 0\end{Bmatrix}\sum_{i=1}^{NG}\sum_{j=1}^{NG}N_i\sqrt{|\boldsymbol{a}|}\omega_i\omega_j \tag{62}$$

### 2.3 Geometric nonlinear formulations of DKMGQ-CR

By introducing the CR method, we present the geometric nonlinear formulations of the new 4-node shell element DKMGQ-CR. CR method has higher accuracy and efficiency than TL (Total Lagrangian) or UL (Updated Lagrangian) method. Furthermore, the geometric linear element formulas can be applied to calculate the internal forces in the co-rotational coordinate system without modification.

#### 2.3.1 Generalized stress-strain and strain-displacement relationship of shell element

Firstly, the stress-strain formula for large rotation and small strain is derived. The material is in the elastic stage in the small strain state, and the stress-strain relationship is linear.

The generalized stress-strain relationship (Zhang *et al.* 2007) is

$$\boldsymbol{\sigma}^*=\boldsymbol{D}^*\boldsymbol{\varepsilon}^* \tag{63}$$

where

$$\boldsymbol{\sigma}^*=[\boldsymbol{N} \quad \boldsymbol{M} \quad \boldsymbol{Q}]^T \tag{64}$$

$$\boldsymbol{D}^*=\begin{bmatrix}\boldsymbol{H_m} & \boldsymbol{0} & \boldsymbol{0}\\ \boldsymbol{0} & \boldsymbol{H_b} & \boldsymbol{0}\\ \boldsymbol{0} & \boldsymbol{0} & \boldsymbol{H_s}\end{bmatrix} \tag{65}$$

$$\boldsymbol{\varepsilon}^*=[\boldsymbol{\varepsilon}_m \quad \boldsymbol{\varepsilon}_b \quad \boldsymbol{\gamma}]^T \tag{66}$$

$$\boldsymbol{N}=[N_x \quad N_y \quad N_{xy}]^T \tag{67}$$

$$\boldsymbol{M}=[M_x \quad M_y \quad M_{xy}]^T \tag{68}$$

$$\boldsymbol{Q}=[Q_x \quad Q_y]^T \tag{69}$$

The internal force of the shell element is shown in Fig. 7. Components of $\boldsymbol{N}$, $\boldsymbol{M}$ and $\boldsymbol{Q}$ in Eq. (64) are not the internal force of the corresponding cross-section but the internal force per unit length of the section.

In geometric nonlinear problems, the strain-displacement relationship is nonlinear. Therefore, the incremental formula is necessary as follows

$$\boldsymbol{\sigma}=\boldsymbol{\sigma}_0+\Delta\boldsymbol{\sigma}=\boldsymbol{\sigma}_0+\boldsymbol{D}^*\Delta\boldsymbol{\varepsilon} \tag{70}$$

The linear strain-displacement relationship is

$$\boldsymbol{\varepsilon}_0=\begin{Bmatrix}\boldsymbol{\varepsilon}_m\\ \boldsymbol{\chi}_b\\ \boldsymbol{\gamma}\end{Bmatrix}=\begin{Bmatrix}\boldsymbol{B}_m\boldsymbol{\delta}_m\\ \boldsymbol{B}_b\boldsymbol{\delta}_p\\ \boldsymbol{B}_s\boldsymbol{\delta}_p\end{Bmatrix}=\begin{bmatrix}\boldsymbol{B_m} & \boldsymbol{0}\\ \boldsymbol{0} & \boldsymbol{B_b}\\ \boldsymbol{0} & \boldsymbol{B_s}\end{bmatrix}\begin{Bmatrix}\boldsymbol{\delta}_m\\ \boldsymbol{\delta}_p\end{Bmatrix}=\boldsymbol{B}_0\boldsymbol{\delta}_{m\text{-}p}^e \tag{71}$$

The strain matrix is a function of displacement $\boldsymbol{\delta}_{m\text{-}p}^e$ in a large deformation problem. By representing the displacement-related parts in the strain matrix by $\boldsymbol{B}_L$, the formula of the strain matrix is

$$\boldsymbol{B}=\boldsymbol{B}_0+\boldsymbol{B}_L \tag{72}$$

The incremental relationship of strain-displacement is

$$\Delta\boldsymbol{\varepsilon}=\boldsymbol{B}\Delta\boldsymbol{\delta}_{m\text{-}p}^e \tag{73}$$

#### 2.3.2 Geometric nonlinear incremental equilibrium equations

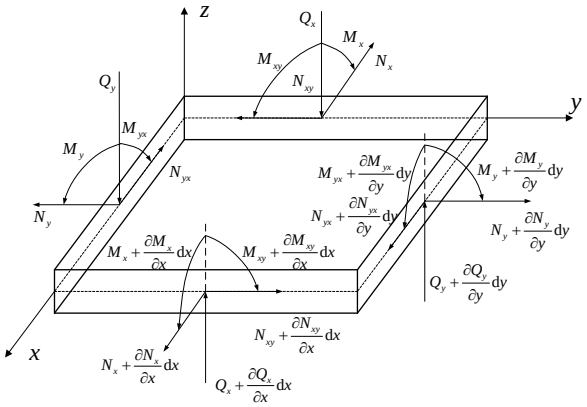


Fig. 7 Internal force of shell element

Based on the principle of virtual work and the incremental relationship of stress-strain and strain-displacement, geometric nonlinear incremental equilibrium equations can be derived.

We define $f_{m\text{-}p}^{e}$ as the resulting force vector of internal and external forces of a node in the local system and define $d\delta_{m\text{-}p}^{e}$ as the virtual displacement of an element in the local system under the current configuration. The principle of virtual work is written as follows

$$\begin{aligned}\left(d\boldsymbol{\delta}_{m\text{-}p}^{e}\right)^{T}\boldsymbol{f}_{m\text{-}p}^{e}=\int d\boldsymbol{\varepsilon}^{T}\,\boldsymbol{\sigma}dA-\left(d\boldsymbol{\delta}_{m\text{-}p}^{e}\right)^{T}\boldsymbol{F}_{m\text{-}p}^{e}=\\ \left(d\boldsymbol{\delta}_{m\text{-}p}^{e}\right)^{T}\left(\int\boldsymbol{B}^{T}\,\boldsymbol{\sigma}dA-\boldsymbol{F}_{m\text{-}p}^{e}\right)=\mathbf{0}\end{aligned}\tag{74}$$

The symbol $(\ )_{m\text{-}p}^{e}$ represents matrix or vector elements in the local system that are sorted according to displacement DOFs of first the membrane and then the plate.

$\left(d\boldsymbol{\delta}_{m\text{-}p}^{e}\right)^{T}$ is eliminated in Eq. (74) to obtain equilibrium equations for general cases, which can apply to large and small deformation.

$$\boldsymbol{f}_{m\text{-}p}^{e}=\int\boldsymbol{B}^{T}\,\boldsymbol{\sigma}dA-\boldsymbol{F}_{m\text{-}p}^{e}=\mathbf{0}\tag{75}$$

Newton-Raphson method is usually used to solve Eq. (75) under geometric large deformation. We take the differential of Eq. (75) and obtain that

$$\begin{aligned}d\boldsymbol{f}_{m\text{-}p}^{e}=\int d\boldsymbol{B}^{T}\boldsymbol{\sigma}dA+\int\boldsymbol{B}^{T}d\boldsymbol{\sigma}\,dA=\int d\boldsymbol{B}_{L}{}^{T}\boldsymbol{\sigma}dA+\\ \bar{\boldsymbol{K}}_{m\text{-}p}^{e}\Delta\boldsymbol{\delta}_{m\text{-}p}^{e}\end{aligned}\tag{76}$$

where

$$\int d\boldsymbol{B}_{L}{}^{T}\boldsymbol{\sigma}dA=(\boldsymbol{K}_{\sigma})_{m\text{-}p}^{e}\Delta\boldsymbol{\delta}_{m\text{-}p}^{e}\tag{77}$$

and

$$\begin{aligned}\bar{\boldsymbol{K}}_{m\text{-}p}^{e}=\int\boldsymbol{B}^{T}\boldsymbol{D}^{*}\boldsymbol{B}\,dA=\int(\boldsymbol{B}_{0}+\boldsymbol{B}_{L})^{T}\boldsymbol{D}^{*}(\boldsymbol{B}_{0}+\\ \boldsymbol{B}_{L})\,dA=(\boldsymbol{K}_{0}+\boldsymbol{K}_{L})_{m\text{-}p}^{e}\end{aligned}\tag{78}$$

where the linear part is

$$(\boldsymbol{K}_{0})_{m\text{-}p}^{e}=\int\boldsymbol{B}_{0}{}^{T}\boldsymbol{D}^{*}\boldsymbol{B}_{0}\,dA\tag{79}$$

and the nonlinear part is

$$(\boldsymbol{K}_{L})_{m\text{-}p}^{e}=\int\boldsymbol{B}_{0}{}^{T}\boldsymbol{D}^{*}\boldsymbol{B}_{L}+\boldsymbol{B}_{L}{}^{T}\boldsymbol{D}^{*}\boldsymbol{B}_{L}+\boldsymbol{B}_{L}{}^{T}\boldsymbol{D}^{*}\boldsymbol{B}_{0}\,dA\tag{80}$$

Then Eq. (76) can be expressed as

$$\Delta\boldsymbol{f}_{m\text{-}p}^{e}=(\boldsymbol{K}_{T})_{m\text{-}p}^{e}\Delta\boldsymbol{\delta}_{m\text{-}p}^{e}\tag{81}$$

After processing the location index, Eq. (76) is written as follows

$$\Delta\boldsymbol{f}^{e}=\boldsymbol{K}_{T}^{e}\Delta\boldsymbol{\delta}^{e}\tag{82}$$

where $K_T^e$ is the local tangent stiffness of the current configuration of the element, as follows

$$\boldsymbol{K}_{T}^{e}=\boldsymbol{K}_{0}^{e}+\boldsymbol{K}_{L}^{e}+\boldsymbol{K}_{\sigma}^{e}\tag{83}$$

where

$\boldsymbol{K}_0^e$ is the material stiffness matrix,

$\boldsymbol{K}_L^e$ is the large displacement matrix,

$\boldsymbol{K}_\sigma^e$ is the geometric stiffness matrix.

Then global tangent stiffness is

$$\boldsymbol{K}_{T}=\sum(\boldsymbol{T}^{T}\boldsymbol{K}_{T}^{e}\boldsymbol{T})\tag{84}$$

where $T$ is the transfer matrix.

The resulting force vector of internal and external forces under the global system is

$$\Delta\boldsymbol{f}=\sum(\boldsymbol{T}^{T}\Delta\boldsymbol{f}^{e})\tag{85}$$

The incremental iterative equation of structure is

$$\Delta\boldsymbol{f}=\boldsymbol{K}_{T}\Delta\boldsymbol{\delta}\tag{86}$$

where $\Delta\boldsymbol{\delta}$ is the global incremental displacement.

### 2.3.3 Algorithms for spatial rotation

The operation rules of small shell rotation are almost the same as vector. However, those operation rules are approximate methods that do not apply to large rotations. The quaternion method is needed to deal with the large rotation of the shell.

The spatial shell element node has six DOFs, ($u$, $v$, $w$, $\theta_x$, $\theta_y$, $\theta_z$), including translational and rotational displacement. During the nonlinear incremental analysis, new translational and rotational displacement increments are obtained at each step, and the corresponding displacement will update after each step. Among them, the translational displacement $\boldsymbol{u}=[u\quad v\quad w]^{T}$ has vector superposition, which can be directly updated by vector addition.

$$\boldsymbol{u}=[u\quad v\quad w]^{T}\tag{87}$$

However, the rotational displacement $\boldsymbol{\omega}=[\theta_x\quad\theta_y\quad\theta_z]^{T}$ cannot be updated directly by addition. The quaternion method is used to store and update rotational displacement. Regard rotational displacement as a "pseudo vector" $\boldsymbol{\omega}$ of spatial rotation, then

$$\boldsymbol{\omega}=\begin{Bmatrix}\theta_x\\ \theta_y\\ \theta_z\end{Bmatrix}=\omega_1\boldsymbol{e}_1+\omega_2\boldsymbol{e}_2+\omega_3\boldsymbol{e}_3=\omega\boldsymbol{e}_r\tag{88}$$

where $\omega_i$ is the rotational component and $\boldsymbol{e}_i$ is the unit base vector of the $i$-th axis of the global coordinate system. The pseudo vector includes the rotation angle $\omega=\|\boldsymbol{\omega}\|=(\omega_1^2+\omega_2^2+\omega_3^2)^{\frac{1}{2}}$ and the direction of rotation $e$. The antisymmetric tensor is

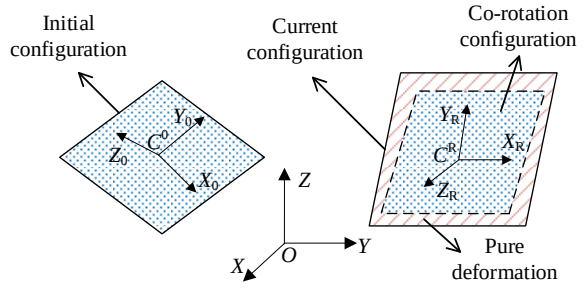


Fig. 8 The coordinate description of co-rotational formulas

$$\boldsymbol{\Omega}(\boldsymbol{\omega}) = \begin{bmatrix} 0 & -\omega_3 & \omega_2 \\ \omega_3 & 0 & -\omega_1 \\ -\omega_2 & \omega_1 & 0 \end{bmatrix} \tag{89}$$

Quaternion $[q_0, q]^{\mathrm{T}}$ (Argyris 1982) is used to calculate the rotational angle, as follows

$$\begin{Bmatrix} q_0 \\ \boldsymbol{q} \end{Bmatrix} = \begin{Bmatrix} q_0 \\ q_1 \\ q_2 \\ q_3 \end{Bmatrix} = \begin{Bmatrix} \cos\frac{\|\boldsymbol{\omega}\|}{2} \\ \frac{\boldsymbol{\omega}}{\|\boldsymbol{\omega}\|}\sin\frac{\|\boldsymbol{\omega}\|}{2} \end{Bmatrix} \tag{90}$$

The initial state is $[\Delta q_0, \Delta \boldsymbol{q}]^T=[1\ 0\ 0\ 0]^T$.

We take an utterly nonsingular rotation matrix $\boldsymbol{R}$ to store and update the rotational angle of large deformation shell elements in the global coordinate system

$$\boldsymbol{R} = 2\begin{bmatrix} q_0^2+q_1^2-\frac{1}{2} & q_1q_2-q_0q_3 & q_1q_3+q_0q_2 \\ q_1q_2+q_0q_3 & q_0^2+q_2^2-\frac{1}{2} & q_2q_3-q_0q_1 \\ q_1q_3-q_0q_2 & q_2q_3+q_0q_1 & q_0^2+q_3^2-\frac{1}{2} \end{bmatrix} \tag{91}$$

In the nonlinear analysis process, if the "pseudo-vector" increment $\Delta\boldsymbol{\omega}$ of the rotation angle is obtained, the quaternion variable $[\Delta\boldsymbol{q}_0, \Delta\boldsymbol{q}]^T$ corresponding to $\Delta\boldsymbol{\omega}$ can be obtained. Then the corresponding incremental rotation matrix $\Delta\boldsymbol{R}$ can be obtained, and the updated rotation matrix can be obtained as follows

$$\boldsymbol{R}_t = \Delta\boldsymbol{R}_t\boldsymbol{R}_{t-1} \tag{92}$$

If the incremental rotation matrix $\Delta R$ is known, the rotational increment can be extracted by second-order approximation

$$\boldsymbol{\Omega}(\Delta\boldsymbol{\omega}) = \frac{2(\Delta\boldsymbol{R}-\Delta\boldsymbol{R}^T)}{1+\mathrm{tr}(\Delta\boldsymbol{R})} \tag{93}$$

where $\mathrm{tr}(\Delta\boldsymbol{R}) = \Delta R_{11} + \Delta R_{22} + \Delta R_{33}$.

### *2.3.4 Pure deformation in Co-rotational coordinate system*

CR method assumes that the element produces rigid body displacement with only a small strain. The calculating of the pure deformation under the current load is most important in the CR method. Then the stiffness and internal force of the shell element in the CR system can be calculated by applying the elastic shell theory directly.

Quadrilateral shell elements' initial configuration, current configuration, and co-rotation configuration are shown in Fig. 8, also known as the co-rotational frame or CR frame (Deng *et al.* 2022, Kan *et al.* 2021).

In initial configuration

$\boldsymbol{X}^g$ is Coordinate of a point, in global system

$\boldsymbol{Q}_R = [r_1^0 \quad r_2^0 \quad r_3^0]$, is transformation matrix of the CR coordinate system $OX_0Y_0Z_0$

$\boldsymbol{X}_0^g$ is coordinate of the origin $C^0$

In current configuration

$\boldsymbol{x}^g$ is coordinate of a point, in global system

$\boldsymbol{Q}_R = [\boldsymbol{r}_1 \quad \boldsymbol{r}_2 \quad \boldsymbol{r}_3]$, is the transformation matrix the CR coordinate system $OX_{\mathrm{R}}Y_{\mathrm{R}}Z_{\mathrm{R}}$

$\boldsymbol{x}_0^g$ is the coordinate of the origin $C^{\mathrm{R}}$

$\boldsymbol{R}^g$ is the overall rotation matrix

$\boldsymbol{u}^g$ is the overall translational displacement matrix

Relative displacement

$\boldsymbol{R}_0^g$ is the rigid rotational displacement

$\boldsymbol{u}_0^g$ is the rigid translational displacement

Therefore, pure deformation is the "pink slash shadow" in Fig. 8.

The pure translation deformation displacement in CR coordinate system is

$$\bar{\boldsymbol{u}}^e = \boldsymbol{x}^e - \boldsymbol{X}^e \tag{94}$$

where

$$\begin{cases} \boldsymbol{X}^e = \boldsymbol{Q}_0^T(\boldsymbol{X}^g - \boldsymbol{X}_0^g) \\ \boldsymbol{x}^e = \boldsymbol{Q}_R^T(\boldsymbol{x}^g - \boldsymbol{x}_0^g) \\ \boldsymbol{x}^g = \boldsymbol{X}^g + \boldsymbol{u}^g \end{cases} \tag{95}$$

The rotation matrix corresponding to the pure rotation deformation displacement in the CR coordinate system is

$$\bar{\boldsymbol{R}}^e = \boldsymbol{Q}_R^T\boldsymbol{R}^g\boldsymbol{Q}_0 \tag{96}$$

where superscript '*e*' indicates the CR coordinate system, and the hat '-' indicates pure deformation. Generally, the pure deformation in the CR coordinate system is small, so the three components of pure rotational displacement can be extracted from Eq.(93).

### *2.3.5 Geometric element stiffness matrix of DKMGQ-CR*

The relationship between pure deformation displacement in the CR coordinate system and the global coordinate system is as follows

$$d\bar{\boldsymbol{\delta}}^e = \bar{\boldsymbol{H}}\bar{\boldsymbol{P}}\boldsymbol{T}d\boldsymbol{\delta}^g \tag{97}$$

where

$d\bar{\boldsymbol{\delta}}^e = [d\bar{\boldsymbol{\delta}}_1^e \quad d\bar{\boldsymbol{\delta}}_2^e \quad d\bar{\boldsymbol{\delta}}_3^e \quad d\bar{\boldsymbol{\delta}}_4^e]^T$ is the incremental form of pure deformation in the CR system of an element, where $d\bar{\boldsymbol{\delta}}_i^e = [d\boldsymbol{u}_i^e \quad d\boldsymbol{\omega}_i^e]^T$ for per node.

$\bar{\boldsymbol{H}}$ is the relationship between the variation of the element pure deformation vector in the CR system and the variation of pure deformation pseudo-vector in the CR system,

$\bar{\boldsymbol{P}}$ is the projection matrix,

$\boldsymbol{T}$ is the transfer matrix,

$d\boldsymbol{\delta}^g = [d\boldsymbol{\delta}_1^g \quad d\boldsymbol{\delta}_1^g \quad d\boldsymbol{\delta}_1^g \quad d\boldsymbol{\delta}_1^g]^T$ is the displacement variation in the global system,

$d\boldsymbol{\delta}_i^g = \left[d\boldsymbol{u}_i^g \quad d\boldsymbol{\omega}_i^g\right]^T$ is the displacement variation in the global system of nodal point *i*.

Definition of $\bar{\boldsymbol{H}}$ is

$$\bar{\boldsymbol{H}} = diag[\boldsymbol{I} \quad \bar{\boldsymbol{H}}_1 \quad \dots \quad \boldsymbol{I} \quad \bar{\boldsymbol{H}}_4] \tag{98}$$

where

$$\bar{\boldsymbol{H}}_i = \frac{\partial \bar{\boldsymbol{\theta}}_i^e}{\partial \bar{\boldsymbol{\omega}}_i^e} = \boldsymbol{I} - \frac{1}{2}\boldsymbol{\Omega}(\bar{\boldsymbol{\theta}}_i^e) + \eta \boldsymbol{\Omega}^2(\bar{\boldsymbol{\theta}}_i^e) \tag{99}$$

and

$$\eta = \frac{1-\frac{1}{2}\theta\, cot\left(\frac{1}{2}\theta\right)}{\theta^2} = \frac{1}{12} + \frac{1}{720}\theta^2 + \frac{1}{30240}\theta^4 + \frac{1}{1209600}\theta^6 + \cdots \tag{100}$$

Matrix $\bar{\boldsymbol{P}}$ is the projection matrix that ensures that the element has accurate rigid body rotation balance and is suitable for element warping.

The expression of $\bar{\boldsymbol{P}}$ is

$$\overline{\boldsymbol{P}} = \boldsymbol{I}_{24} - \overline{\boldsymbol{SG}} \tag{101}$$

where

$$\bar{\boldsymbol{G}} = \begin{bmatrix} 0 & 0 & 1/\beta \\ 0 & 0 & 0 \\ -x_2^e/\alpha_0 & (y_4^e - y_2^e)/\alpha_0 & z_4^e(y_4^e - y_2^e)/(\alpha_0\beta) \\ & \boldsymbol{0}_{3\times3} & \\ 0 & 0 & 0 \\ 0 & 0 & 0 \\ -x_3^e/\alpha_0 & -y_3^e/\alpha_0 & z_4^e y_3^e/(\alpha_0\beta) \\ & \boldsymbol{0}_{3\times3} & \\ 0 & 0 & 0 \\ 0 & 0 & 0 \\ x_2^e/\alpha_0 & -(y_4^e - y_2^e)/\alpha_0 & -z_4^e(y_4^e - y_2^e)/(\alpha_0\beta) \\ & \boldsymbol{0}_{3\times3} & \\ 0 & 0 & 0 \\ 0 & 0 & 0 \\ x_3^e/\alpha_0 & y_3^e/\alpha_0 & z_4^e y_3^e/(\alpha_0\beta) \\ & \boldsymbol{0}_{3\times3} & \end{bmatrix} \tag{102}$$

$$\bar{\boldsymbol{S}} = [\bar{\boldsymbol{S}}_1 \quad \boldsymbol{I} \quad \cdots \quad \bar{\boldsymbol{S}}_4 \quad \boldsymbol{I}]^T, \bar{\boldsymbol{S}}_i = \boldsymbol{\Omega}(\boldsymbol{x}_i^e) \tag{103}$$

For linear elastic problems, the element internal force vector $\bar{\boldsymbol{f}}^e$ in the CR coordinate system is

$$\bar{\boldsymbol{f}}^e = \bar{\boldsymbol{K}}^e \bar{\boldsymbol{\delta}}^e \tag{104}$$

Then the internal force of the element in the global system is

$$\boldsymbol{f}^e = \boldsymbol{T}^T \bar{\boldsymbol{P}}^T \bar{\boldsymbol{H}}^T \bar{\boldsymbol{f}}^e \tag{105}$$

The tangent stiffness of an element in the global system is

$$\boldsymbol{K}'_T = \boldsymbol{T}^T(-\bar{\boldsymbol{F}}_{\mathrm{nm}}\bar{\boldsymbol{G}} - \bar{\boldsymbol{G}}\bar{\boldsymbol{F}}_n^T\bar{\boldsymbol{P}} + \bar{\boldsymbol{P}}^T\bar{\boldsymbol{L}}\bar{\boldsymbol{P}} + \bar{\boldsymbol{P}}^T\bar{\boldsymbol{H}}^T\bar{\boldsymbol{K}}^e\bar{\boldsymbol{H}}\bar{\boldsymbol{P}})\boldsymbol{T} \tag{106}$$

where

$$\bar{\boldsymbol{F}}_{\mathrm{nm}} = \begin{bmatrix} \boldsymbol{\Omega}(\bar{\boldsymbol{n}}_1^e) \\ \boldsymbol{\Omega}(\bar{\boldsymbol{m}}_1^e) \\ \vdots \\ \boldsymbol{\Omega}(\bar{\boldsymbol{n}}_4^e) \\ \boldsymbol{\Omega}(\bar{\boldsymbol{m}}_4^e) \end{bmatrix}, \qquad \begin{bmatrix} \bar{\boldsymbol{n}}_1^e \\ \bar{\boldsymbol{m}}_1^e \\ \vdots \\ \bar{\boldsymbol{n}}_4^e \\ \bar{\boldsymbol{m}}_4^e \end{bmatrix} = \bar{\boldsymbol{P}}^T\bar{\boldsymbol{H}}^T\bar{\boldsymbol{f}}^e \tag{107}$$

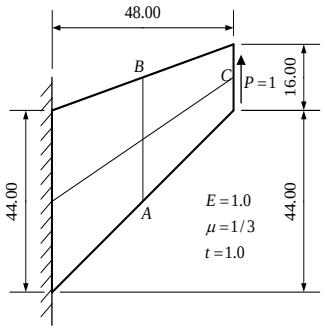


Fig. 9 Cook's problem (2×2 meshes)

$$\bar{\boldsymbol{F}}_n^T = -[\boldsymbol{\Omega}(\bar{\boldsymbol{n}}_1^e) \quad \boldsymbol{0} \quad \dots\cdots \quad \boldsymbol{\Omega}(\bar{\boldsymbol{n}}_4^e) \quad \boldsymbol{0}] \tag{108}$$

$$\bar{\boldsymbol{L}} = diag[\boldsymbol{0} \quad \bar{\boldsymbol{L}}_1 \quad \dots \quad \boldsymbol{0} \quad \bar{\boldsymbol{L}}_4] \tag{109}$$

$$\bar{\boldsymbol{L}}_i = \left\{\eta\left[(\bar{\boldsymbol{\theta}}_i^{\mathrm{eT}}\bar{\boldsymbol{f}}_{mi}^e)\boldsymbol{I} + \bar{\boldsymbol{\theta}}_i^e(\bar{\boldsymbol{f}}_{mi}^e)^T - 2\bar{\boldsymbol{f}}_{mi}^e\bar{\boldsymbol{\theta}}_i^{\mathrm{eT}}\right] + \mu\boldsymbol{\Omega}^2(\bar{\boldsymbol{\theta}}_i^e)\bar{\boldsymbol{f}}_{mi}^e\bar{\boldsymbol{\theta}}_i^{\mathrm{eT}} - \frac{1}{2}\boldsymbol{\Omega}(\bar{\boldsymbol{f}}_{mi}^e)\right\}\bar{\boldsymbol{H}}_i \tag{110}$$

where $\bar{f}_{mi}^e$ is the moment sub-vector of 3×1 corresponding to the *i*-th node in the element's internal force vector, as follows

$$\bar{\boldsymbol{f}}_{mi}^e = \bar{\boldsymbol{m}}_i^e = \left[\bar{M}_{ix}^e \quad \bar{M}_{iy}^e \quad \bar{M}_{iz}^e\right]^T \tag{111}$$

And $\mu$ is defined as

$$\mu = \frac{1}{360} + \frac{1}{7560}\theta^2 + \frac{1}{201600}\theta^4 + \frac{1}{5987520}\theta^6 + \dots \tag{112}$$

The tangent stiffness of an element in the global system $\boldsymbol{K}'_T$ is not symmetrical. The efficiency of existing linear matrix algorithms for large sparse asymmetric matrices is significantly lower than that of symmetric matrices. Therefore, a symmetrical stiffness matrix is necessary. The following symmetrical element tangent stiffness matrix can be applied to the practical calculation

$$\boldsymbol{K}_T = \frac{1}{2}(\boldsymbol{K}'_T + (\boldsymbol{K}'_T)^T) \tag{113}$$

## 3. Numerical tests

### *3.1 Classical plane stress elastic problem*

In the plane stress elastic problem, elements are in the two-dimensional plane, and the forces are also in the same plane. These problems are mainly used to test the performance of the membrane behavior of shell elements.

#### *3.1.1 Cook's beam problem*

Cook's beam problem is a standard benchmark to test the deformation behavior of planar stress membrane elements. We test the in-plane bending and shearing behaviors of the element DKMGQ-CR through the solution to Cook's problem. The irregular cantilever trapezoidal beam model with 2×2 mesh is subjected to shear force P at the right end, as shown in Fig. 9.

We consider the vertical displacement of point C under

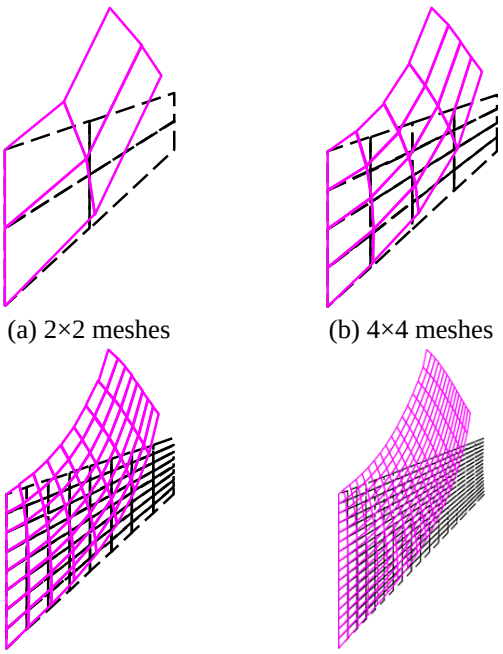

(a) 2×2 meshes (b) 4×4 meshes

(c) 8×8 meshes (d) 16×16 meshes

Fig. 10 Deformed shapes of Cook's beam

Table 1 The vertical displacement of point C in Cook's problem

| Element | Mesh | | | |
|---|---|---|---|---|
| | 2×2 | 4×4 | 8×8 | 16×16 |
| DKMGQ-CR | 21.27 | 23.08 | 23.67 | 23.87 |
| GQ12 (Long *et al.* 2009, Xu and Long 1993) | 20.89 | 23.06 | 23.67 | —— |
| GQ12 (Gao *et al.* 2016) | 21.27 | 23.07 | 23.67 | —— |
| Thick shell in SAP2000 | 20.50 | 22.73 | 23.58 | 23.84 |
| Reference solution | 23.96 | | | |

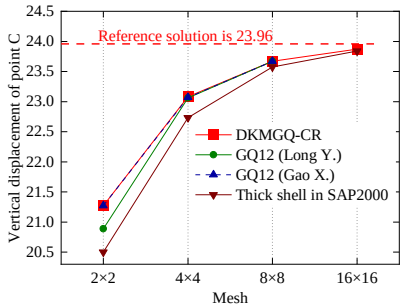


Fig. 11 Results of Cook's problem

meshes of 2×2, 4×4, 8×8 and 16×16 elements, as shown in Fig. 10. The results from DKMGQ-CR and other types of elements are given in Table 1 for comparison.

A comparison of calculation results between the DKMGQ-CR shell and other elements is shown in Fig. 11. DKMGQ-CR shell has high precision in calculating the deformation model of the membrane. For all kinds of elements shown in Fig. 11, finer meshes give more precise results. The calculated results of DKMGQ-CR are consistent with those of the improved GQ12 membrane (Gao *et al.* 2016). The membrane in the DKMGQ-CR shell element has improved the establishment of its local coordinate system based on the GQ12 membrane (Xu and Long 1993), so the calculation accuracy is slightly higher, especially in the cases of 2×2 and 4×4 meshes.

Cook's beam is an irregular trapezoidal beam. Irregular elements exist no matter how meshes are divided. Therefore, the mesh distortion sensitivity of the element can be well verified. DKMGQ-CR shell shows good performance in the distorted mesh model.

### *3.1.2 MacNeal's beam problem*

MacNeal's beam problem (Macneal and Harder 1985) is a classic benchmark to test the ability to eliminate the membrane locking of an element.

The left end of MacNeal's beam is fixed, and the right end is subjected to unit shear load and moment, as shown in Fig. 12. There are generally three ways of meshing: rectangular (a), trapezoidal (b) and parallelogram (c). The results of MacNeal's beam under unit shear load are shown in Table 2.

The results of the DKMGQ-CR shell are not strictly consistent under three different meshes. The results under mesh (a) are the most accurate, indicating that regular mesh gives precise results. The results have no more than 15 percent deviations under distorted mesh (b) and (c). The results of the DKMGQ-CR shell are in good agreement with those of the improved GQ12 membrane (Gao *et al.* 2016), and the results are better than those of the early GQ12 membrane (Long and Xu 1994a, Xu and Long 1993). Furthermore, the DKMGQ-CR and the improved GQ12 show better performance than the classical bilinear element Q4. The results of Q4 have been taken from the study of Gao et al (Gao *et al.* 2016).

The DKMGQ-CR shell element shows low sensitivity in mesh distortion in Cook's beam problem. The results of MacNeal's beam show that the DKMGQ-CR effectively alleviates membrane locking.

### *3.2 Square plate under uniform load problem*

The square plate under uniform load is shown in Fig. 13. The four sides of the plate are fixed. This test analyses the mesh distortion sensitivity of a 4-node plate element (Katili *et al.* 2015a). Due to the symmetry of this plate, 1/4 plate (ABCD shadow part) is used to be analyzed.

Boundary conditions are:

Side AB: $u = v = w = \theta_x = \theta_z = 0$

Side AD: $u = v = w = \theta_y = \theta_z = 0$

Side BC: $u = \theta_y = \theta_z = 0$

Side CD: $v = \theta_x = \theta_z = 0$

The reference solution of deflection of point C is $w_C = 62.830$.

We take three kinds of meshes (a), (b), and (c) to divide a square plate, as shown in Fig. 14 for 2×2 mesh and Fig. 15 for 8×8 mesh. Mesh (a) is rectangular, while meshes (b) and (c) are irregular quadrilaterals. Irregularity of mesh (b) is between that of meshes (a) and (c). In addition to 2×2 meshes, we also take 4×4, 8×8 and 16×16 meshes.

Table 3 shows the typical deflection of point C of three

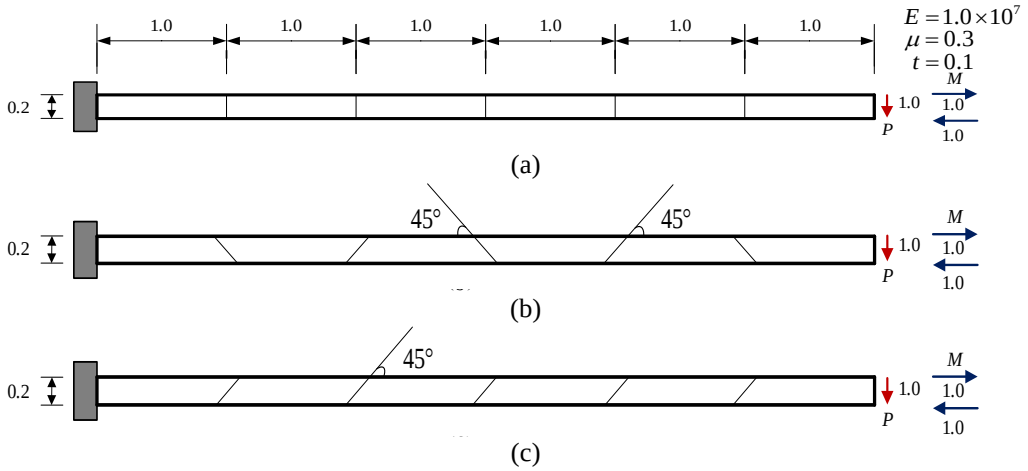


Fig. 12 Three kinds of the mesh of MacNeal's beam, (a) Rectangular, (b) Trapezoidal and (c) Parallelogram

Table 2 Results of MacNeal's beam problem

| Element | Load P (Shear force) | | | Load M (Moment) | | |
|---|---|---|---|---|---|---|
| | Mesh (a) | Mesh (b) | Mesh (c) | Mesh (a) | Mesh (b) | Mesh (c) |
| DKMGQ-CR | -0.0977 | -0.0871 | -0.0944 | -0.0049 | -0.0044 | -0.0048 |
| GQ12 (Long and Xu 1994a, Xu and Long 1993) | -0.0904 | -0.0767 | -0.0860 | —— | —— | —— |
| GQ12 (Gao *et al.* 2016) | -0.0977 | -0.0871 | -0.0944 | —— | —— | —— |
| Q4 | -0.0904 | -0.0710 | -0.0800 | —— | —— | —— |
| Reference solution (Macneal and Harder 1985) | | -0.1081 | | | -0.0054 | |

shell elements, including DKMGQ-CR, TMQ (Cen *et al.* 1999) and DKMQ24 (Katili *et al.* 2015a). The results indicate that the DKMGQ-CR can converge to the reference solution under all listed thickness-span ratios and meshes.

The normalized results of the square plate problem with the span-thickness ratio of 0.1 are shown in Fig. 16. Since DKMGQ-CR and DKMQ24 (Katili *et al.* 2015a) are based on DKMQ plate element, they behave consistently under mesh (c). Although the DKMGQ-CR shell shows the highest accuracy under mesh (a), it shows the lowest accuracy under mesh (c). As the mesh becomes finer, the results under meshes (a), (b), and (c) of DKMGQ-CR are all converge to the reference solution. The results show that the DKMGQ-CR shell has high accuracy and is relatively not sensitive to mesh distortion.

The normalized results of the square plate problem with different thickness-span ratios under mesh (a) are shown in Fig. 17. The results of DKMGQ for shells with different thickness-span ratios are consistent with the reference solution. The reason is that the plate part of the DKMGQ-CR shell considers the shear effect based on Mindlin's thick plate theory. However, the corresponding calculation error of the DKMGQ-CR does not exceed 5%

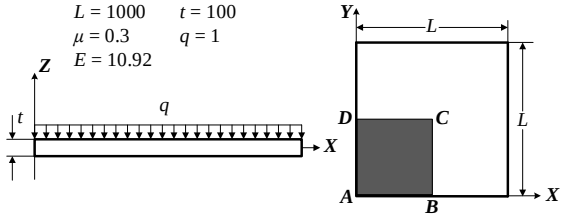


Fig. 13 Four-sided clamped support square plate subjected to uniform load

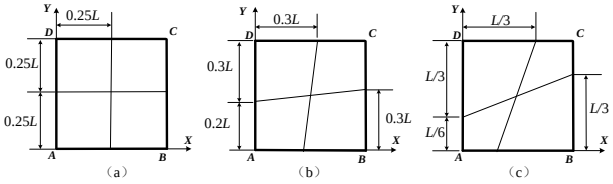


Fig. 14 Three different 2×2 meshes of a square plate

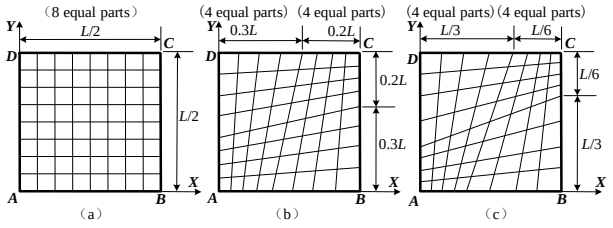


Fig. 15 Three different 8×8 meshes of square plate

when the thickness-span ratio is small to 0.01 and the mesh is 4×4 under mesh (a). The accuracy of DKMGQ-CR and TMQ is highly consistent when the thickness-span ratio is 0.1. The analysis shows that the DKMGQ-CR suits thick and thin shells with high calculation accuracy.

### *3.3 Razzaque skew plate problem*

Razzaque skew plate (Razzaque 1973) and its parameters are shown in Fig. 18. Razzaque plate has the "bridge-type" boundary condition. One pair of opposite sides (AB and CD) is simply supported, and the other pair (AD and BC) is free. The whole plate is

Table 3 Typical deflection of point C with different *t/L* and meshes

| Shell element | Thickness-span ratio *t/L* | Mesh | Deflection typical value of point C | | | | Reference solution $\left(w_C \times \frac{G}{tq}\right)$ |
|---|---|---|---|---|---|---|---|
| | | | 2×2 mesh | 4×4 mesh | 8×8 mesh | 16×16 mesh | |
| DKMGQ-CR | 0.01 | (a) | 614376 | 555114 | 538188 | 533862 | 531300 (Cen *et al.* 1999) |
| | | (b) | 673890 | 569604 | 541800 | 534786 | |
| | | (c) | 715680 | 581658 | 544908 | 535542 | |
| | 0.05 | (a) | 1017.744 | 924.588 | 899.472 | 893.676 | 890.3 (Srinivas and Rao 1973) |
| | | (b) | 1112.244 | 947.688 | 905.184 | 895.104 | |
| | | (c) | 1177.848 | 966.168 | 909.720 | 896.112 | |
| | 0.1 | (a) | 70.5436 | 65.0335 | 63.6327 | 63.3017 | 62.830 (Srinivas and Rao 1973) |
| | | (b) | 76.3388 | 66.4256 | 63.9764 | 63.3870 | |
| | | (c) | 80.2548 | 67.4752 | 64.2266 | 63.4472 | |
| | 0.2 | (a) | 6.1685 | 5.8194 | 5.7311 | 5.7092 | 5.688 (Cen *et al.* 1999) |
| | | (b) | 6.5187 | 5.9022 | 5.7516 | 5.7143 | |
| | | (c) | 6.7456 | 5.9612 | 5.7663 | 5.7180 | |
| | 0.3 | (a) | 1.7969 | 1.7113 | 1.6901 | 1.6848 | 1.673 (Cen *et al.* 1999) |
| | | (b) | 1.8670 | 1.7283 | 1.6943 | 1.6858 | |
| | | (c) | 1.9150 | 1.7409 | 1.6975 | 1.6867 | |
| TMQ (Cen *et al.* 1999) | 0.1 | (a) | 70.476 | 65.016 | 63.630 | 63.294 | 62.830 (Srinivas and Rao 1973) |
| | | (b) | 76.440 | 66.486 | 64.008 | 63.378 | |
| | | (c) | 80.514 | 67.578 | 64.260 | 63.462 | |
| DKMQ24 (Katili *et al.* 2015a) | 0.1 | (c) | 80.653 | 67.876 | 64.596 | 63.798 | 62.830 (Srinivas and Rao 1973) |

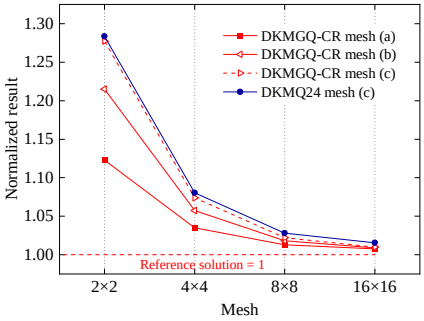


Fig. 16 Normalized results of square plate problem with thickness-span ratio=0.1

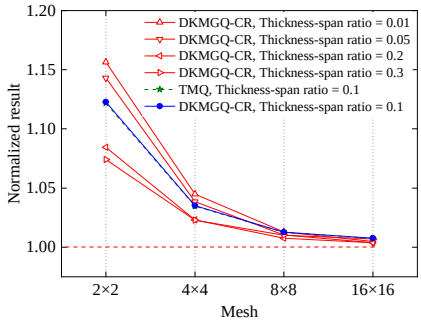


Fig. 17 Normalized results of square plate problem under mesh (a)

subjected to a uniform surface load.

The solutions to the Razzaque skew plate problem under different mesh are shown in Table 4 and Fig. 19. In this

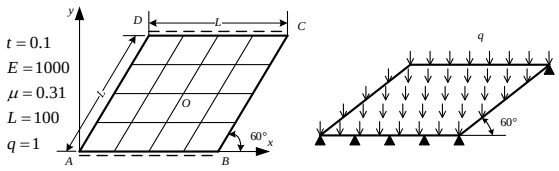


Fig. 18 Razzaque skew plate

problem, a comparison is made among six kinds of shell elements, proposed DKMGQ-CR shell element, ASQ-I (Wang *et al.* 2010), ATF-BQ4 (results taken from the study of Wang et.al (Wang *et al.* 2010)) ,DKMQ (Katili 1993), MITC4 (Bathe and Dvorkin 1985), and the thick shell in SAP2000. The accuracy of DKMGQ-CR is higher than the that of other five types of elements under 6×6, 8×8, and 16×16 meshes. The accuracy of DKMGQ-CR is significantly higher than that of ATF-BQ4, DKMQ, MITC4, and thick shell in SAP2000 under the coarse mesh. This problem indicates that DKMGQ-CR can significantly reduce the influence of distorted meshes in both coarse and fine mesh.

### *3.4 Pinched cylinder problem*

In the problem of the pinched cylinder (Belytschko and Leviathan 1994, Lu *et al.* 2017), the elements are in three-dimensional space. The element has both membrane and plate deformation under loads in this case. A pinched cylinder and its parameters are shown in Fig. 20. A pair of concentrated forces act on the side center of a cylindrical

Table 4 Normalized results of Razzaque skew plate problem

| Element | Mesh | | | | |
|---|---|---|---|---|---|
| | 2×2 | 4×4 | 6×6 | 8×8 | 16×16 |
| DKMGQ-CR | 0.892 | 0.976 | 0.989 | 0.994 | 0.997 |
| ASQ-I (Wang *et al.* 2010) | 0.952 | 0.979 | 0.988 | 0.992 | 0.996 |
| ATF-BQ4 | 1.239 | 1.081 | 1.034 | 1.022 | 1.005 |
| DKMQ (Katili, 1993) | 0.839 | 0.969 | 0.985 | 0.991 | —— |
| MITC4 (Bathe and Dvorkin 1985) | 0.500 | 0.848 | 0.928 | 0.958 | —— |
| Thick shell in SAP2000 | 0.761 | 0.919 | 0.961 | 0.977 | 0.993 |
| Finite difference solution (Razzaque 1973) | | | 1.000* | | |

* The finite difference solution is 0.7945.

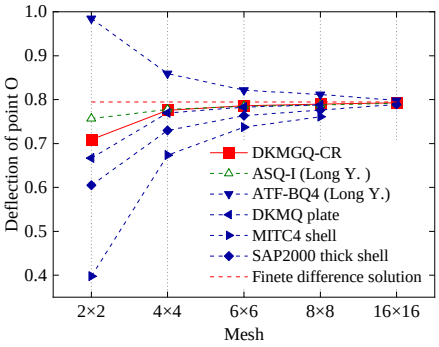


Fig. 19 Results of Razzaque skew plate problem

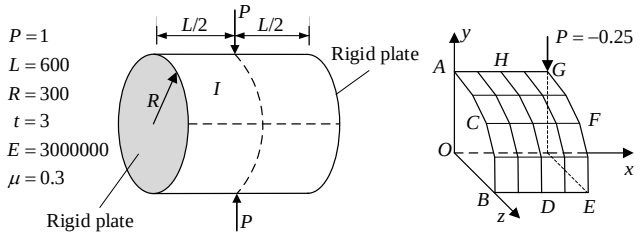


Fig. 20 Pinched cylinder with rigid constraints at both ends

shell with rigid partitions at both ends to verify the shell element's in-plane and out-of-plane coupled state performance. The theoretical solution of load point displacement is $\omega = 1.8541 \times 10^{-5}$.

We can just analyze the 1/8 structure due to the symmetry of the cylindrical structure and the load form. The calculated solutions of the loading point along the loading direction are listed in Table 5.

The normalized solutions are shown in Fig. 21 to intuitively display the variation trend of solution accuracy with different meshes. As shown in Fig. 21, solutions of the DKMGQ-CR shell quickly approach the theoretical solution with the mesh refinement, consistent with solutions of the NLDKGQ shell (Lu *et al.* 2017) and DKMQ24 (Katili *et al.* 2015a) shell. Moreover, the accuracy of DKMGQ-CR is higher than that of GCR24, DKGQ, and the thin and thick shells in SAP2000. Solutions to the pinched cylinder problem demonstrate that DKMGQ-CR is highly suitable for comprehensive deformation analysis coupled with plate and membrane deformation.

### *3.5 Large deformation problem of a slender cantilever beam*

The previous five problems are used to test the linear analysis performance of the DKMGQ-CR shell, and the following two problems are used to test its geometric nonlinear analysis performance. The slender cantilever beam is shown in Fig. 22. We analyze two cases, where (a) is the concentrated bending moment at the end of the beam (Arciniega and Reddy 2007a, 2007b, Gutierrez *et al.* 2016, Ko *et al.* 2017b, Li and Zhan 2000, Lu *et al.* 2017, Moita *et al.* 2016, Schulz and Filippou 2001, Sze *et al.* 2004, Yoon and Lee 2014) and (b) is the concentrated shear force at the end of the beam (Arciniega and Reddy 2007a, Gutierrez *et al.* 2016, Lu *et al.* 2017, Sze *et al.* 2004). The left end of the beam is fixed.

In case (a), the large deformation of the beam will produce a circular arc configuration according to the elastic beam theory. The circular arc radius is $R=EI/M$, where $I=bh^3/12$ (Schulz and Filippou 2001).

We mesh the beam into ten elements along the length direction. The theoretical relation of the force-displacement curve can be derived from the bending moment-curvature relation as follows

$$u = \frac{L}{2\pi\lambda} sin\, 2\pi\lambda - L \quad w = \frac{L}{2\pi\lambda}(1 - cos\, 2\pi\lambda) \qquad (114)$$

where

$\lambda = M/M_{\max}$ ,

$M_{\max} = 2\pi EI/L$.

The change of configuration with the bending moment is shown in Fig. 23. The slender cantilever beam forms

a complete circle when $M=M_{\max}$,

a 3/4 circle when $M=0.75M_{\max}$,

a 1/2 circle when $M=0.5M_{\max}$,

a 1/4 circle when $M=0.25M_{\max}$.

The calculated results are consistent with the theoretical values in these typical configurations.

The load-displacement curve of the slender cantilever beam under bending moment is shown in Fig. 24. The symbol $u$ represents the displacement of the loading point in the $x$-direction, and $w$ represents the displacement in the $z$-direction. As shown in Fig. 24, the load-displacement curves in $x$ and $z$ directions are highly consistent with the

Table 5 Normalized results of the pinched cylinder with diaphragm problem

| Shell element | Mesh | | |
|---|---|---|---|
| | 4×4 | 8×8 | 16×16 |
| DKMGQ-CR | 0.629 | 0.938 | 1.005 |
| NLDKGQ in Opensees (Lu *et al.* 2017) | 0.629 | 0.935 | 0.999 |
| DKMQ24(Katili *et al.* 2015a) | 0.607 | 0.930 | 1.003 |
| GCR24(Long and Xu 1994b) | 0.610 | 0.895 | 0.968 |
| DKGQ(Wang *et al.* 2016) | 0.629 | 0.789 | 0.930 |
| Thick shell in SAP2000 | 0.630 | 0.656 | 0.670 |
| Thin shell in SAP2000 | 0.405 | 0.623 | 0.662 |
| Theoretical solution (Belytschko and Leviathan 1994) | | 1.000* | |

*The theoretical solution is $1.8541\times10^{-5}$

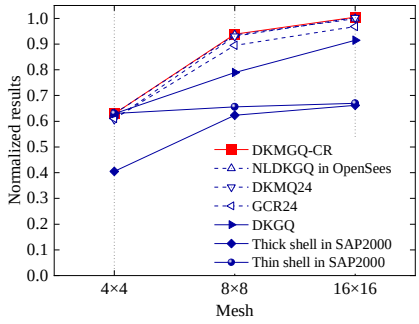


Fig. 21 Normalized results of pinched cylinder problem

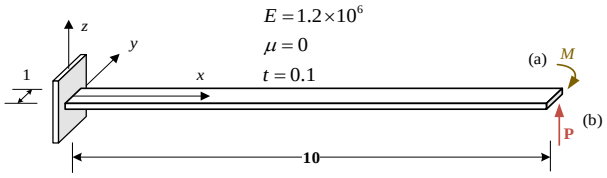


Fig. 22 Slender cantilever beam with (a) Bending moment and (b) Shear force

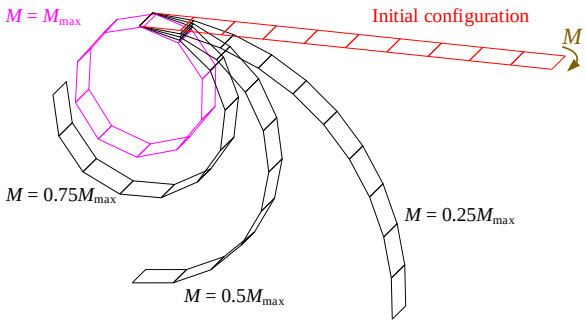


Fig. 23 Bending deformation the shape of slender cantilever beam

theoretical results.

In case (b) of Fig. 22, the left end of the slender cantilever beam is fixed, and the right end is loaded by shear force $P$. There is no theoretical solution for case (b). Researchers usually consider the maximum shear load $P_{max}$ $=4EI/L$, where $I=bh^3/12$.

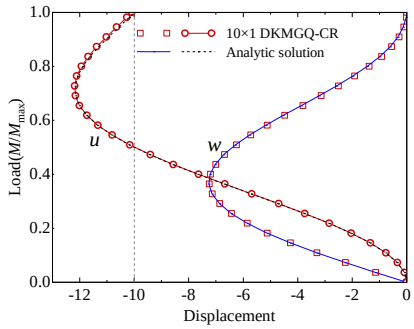


Fig. 24 Load-displacement curve of the slender cantilever beam under bending moment

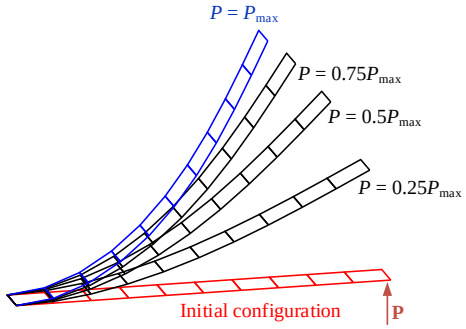


Fig. 25 Shear deformation shape of the slender cantilever beam

The shear deformation diagram of the slender cantilever beam where the corresponding $P$ equals 0, $0.25P_{max}$, $0.5P_{max}$, $0.75P_{max}$ and $P_{max}$ is shown in Fig. 25.

The load-displacement curve of the slender cantilever beam under shear force is shown in Fig. 26. The symbol $u$ represents the displacement of the loading point in the $x$-direction, and $w$ represents the displacement in the $z$-direction. As shown in Fig. 26, the load-displacement curves under shear force $P$ of shell element DKMGQ-CR are highly consistent with the solutions of S4R in Abaqus and the thick shell in SAP2000.

The results of the cantilever beam problem show that the DKMGQ-CR shell for large deformation can accurately simulate the large rotational deformation of the shells.

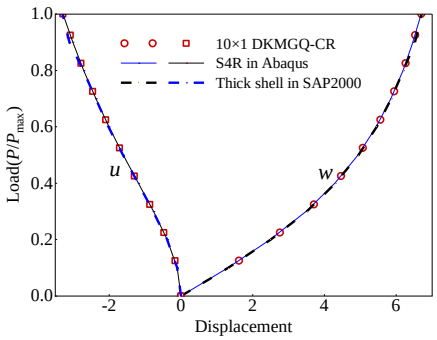


Fig. 26 Load-displacement curve of the cantilever beam under shear force

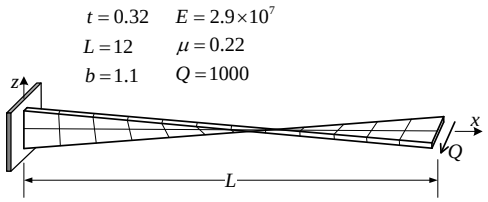


Fig. 27 Twisted cantilever beam

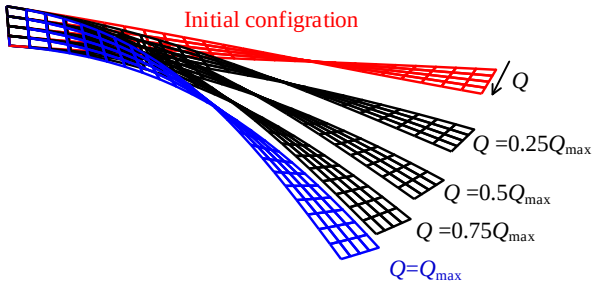


Fig. 28 Shear deformation shape of the twisted cantilever beam

### *3.6 Large deformation problem of a twisted cantilever beam*

The twisted cantilever beam problem is a classic benchmark to test the large deformation capacity of shell elements (Katili *et al.* 2015a, Kim *et al.* 2007, Ko *et al.* 2017b, Yoon and Lee, 2014). The twisted cantilever beam is uniformly twisted by 90° from the fixed end to the free end, as shown in Fig. 27. The left end of the beam is fixed, and the right end is free. The free end is applied concentrated load $Q$. The maximum value of the load is $Q_{max}$=1000. We take meshes of 4×24 to calculate the displacement of the loading point.

The shear deformation diagram of the twisted cantilever beam where the corresponding $Q$ equals 0, $0.25Q_{max}$, $0.5Q_{max}$, $0.75Q_{max}$ and $Q_{max}$ is shown in Fig. 28.

The load-displacement curve of the twisted cantilever beam under concentrated load $Q$ is shown in Fig. 29. The curve of results derived from the DKMGQ-CR shell for large deformation is consistent with the results of thick shell and thin shell in SAP2000.

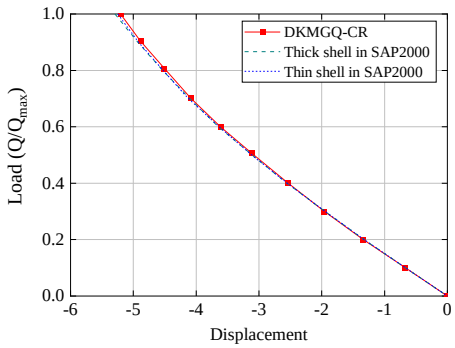


Fig. 29 Load-displacement curve of the twisted beam under shear force

## 4. Conclusions

This paper proposed a high-performance shell element DKMGQ-CR with four nodes and 24 DOFs based on generalized conforming theory, discrete Kirchhoff plate theory, Reissner-Mindlin theory, and co-rotational formulation. The new element is suitable for geometric nonlinear analysis by introducing the Co-rotational formulation. The linear and nonlinear performance of the proposed shell element was validated through the numerical testing of various classical and strict benchmark examples. The advantages of the above element construction theory are well combined. Hence the DKMGQ-CR element has high precision, concise formulations, good capacity for resisting various mesh distortions, and versatility for shells of different thicknesses without locking. This high-performance flat shell element DKMGQ-CR is expected to provide an accurate and convenient tool for the geometric nonlinear analysis of shells in related research fields.

## Acknowledgments

This research was funded by the National Natural Science Foundations of China (Grant No. 51921006 and 51978224), the National Major Scientific Research Instrument Development Program of China (Grant No. 51827811), the Natural Science Foundation of Guangdong Province (Grant No. 2022A1515010403), the Shenzhen Technology Innovation Program (Grant No. JCYJ20180508152238111 and JCYJ20200109112803851), and the Shenzhen Sustainable Development Project (Grant No. KCXFZ202002011010039 and KCXFZ20200121090659756).

## References

Arciniega, R.A. and Reddy, J.N. (2007a), "Tensor-based finite element formulation for geometrically nonlinear analysis of shell structures", *Comput. Method. Appl. Mech. Eng.*, **196**(4-6), 1048-1073. https://doi.org/10.1016/j.cma.2006.08.014.

Arciniega, R.A. and Reddy, J.N. (2007b), "Large deformation analysis of functionally graded shells", *Int. J. Solid. Struct.*, **44**(6), 2036-2052. https://doi.org/10.1016/j.ijsolstr.2006.08.035.

Argyris, J. (1982), "An excursion into large rotations", *Comput. Method. Appl. Mech. Eng.*, **32**(1-3), 85-155. https://doi.org/10.1016/0045-7825(82)90069-x.

Attia, S., Mohareb, M., Martens, M., Ghodsi, N.Y., Li, Y. and Adeeb, S. (2022), "Shell finite element formulation for geometrically nonlinear analysis of curved thin-walled pipes", *Thin Wall. Struct.*, **173**, 108971. https://doi.org/10.1016/j.tws.2022.108971.

Bathe, K.J. and Dvorkin, E.N. (1985), "A 4-node plate bending element based on Mindlin reissner plate-theory and a mixed interpolation", *Int. J. Numer. Method. Eng.*, **21**(2), 367-383. https://doi.org/10.1002/nme.1620210213.

Batoz, J.L., Bathe, K.Jür. and Ho, L.W. (1980), "A study of three-node triangular plate bending elements", *Int. J. Numer. Method. Eng.*, **15**(12), 1771-1812. https://doi.org/10.1002/nme.1620151205.

Battini, J.M. and Pacoste, C. (2006), "On the choice of the linear element for corotational triangular shells", *Comput. Method. Appl. Mech. Eng.*, **195**(44), 6362-6377. https://doi.org/10.1016/j.cma.2006.01.007.

Belytschko, T. and Leviathan, I. (1994), "Physical stabilization of the 4-node shell element with one-point quadrature", *Comput. Method. Appl. Mech. Eng.*, **113**(3-4), 321-350. https://doi.org/10.1016/0045-7825(94)90052-3.

Bisegna, P., Caruso, G., Caselli, F. and Nodargi, N.A. (2017), "A corotational triangular facet shell element for geometrically nonlinear analysis of thin piezoactuated structures", *Compos. Struct.*, **172**, 267-281. https://doi.org/10.1016/j.compstruct.2017.03.074.

Bucalem, M.L. and Bathe, K.J. (1993), "Higher-order MITC general shell elements", *Int. J. Numer. Method. Eng.*, **36**(21), 3729-3754. https://doi.org/10.1002/nme.1620362109.

Cen, S., Long, Z. and Long, Y. (1999), "A Mindlin quadrilateral plate element with improved interpolation for the rotation and shear fields", *Eng. Mech.*, **16**(4), 1-15.

Cen, S., Wu, C.J., Li, Z., Shang, Y. and Li, C. (2019), "Some advances in high-performance finite element methods", *Eng. Comput.*, **36**(8), 2811-2834. https://doi.org/10.1108/EC-10-2018-0479.

Cho, H., Kim, H. and Shin, S. (2018), "Geometrically nonlinear dynamic formulation for three-dimensional co-rotational solid elements", *Comput. Method. Appl. Mech. Eng.*, **328**, 301-320. https://doi.org/10.1016/j.cma.2017.08.037.

Choi, C.K. and Lee, T.Y. (2003), "Efficient remedy for membrane locking of 4-node flat shell elements by non-conforming modes", *Comput. Method. Appl. Mech. Eng.*, **192**(16), 1961-1971. https://doi.org/10.1016/S0045-7825(03)00203-2.

Crisfield, M.A. (1984), "A quadratic Mindlin element using shear constraints", *Comput. Struct.*, **18**(5), 833-852. https://doi.org/10.1016/0045-7949(84)90030-0.

Deng, L., Niu, M., Xue, J. and Chen, L. (2023), "An ALE formulation for the geometric nonlinear dynamic analysis of planar curved beams subjected to moving loads", *Mech. Syst. Signal Pr.*, **184**, 109670. https://doi.org/10.1016/j.ymssp.2022.109670.

Deng, L., Zhang, Y. and Chen, L. (2022), "An arbitrary Lagrangian-Eulerian formulation of two-dimensional viscoelastic beams based on the consistent corotational method", *J. Comput. Nonlinear Dyn.*, **17**(7), 071001. https://doi.org/10.1115/1.4053992.

Dvorkin, E.N. and Bathe, K.J. (1984), "A continuum mechanics based four-node shell element for general non-linear analysis", *Eng. Comput.*, **1**(1), 77-88. https://doi.org/10.1108/eb023562.

Felippa, C.A. and Haugen, B. (2005), "A unified formulation of small-strain corotational finite elements: I. Theory", *Comput. Method. Appl. Mech. Eng.*, **194**(21-24), 2285-2335. https://doi.org/10.1016/j.cma.2004.07.035.

Gao, X., Liu, Y. and Lv, J. (2016), "A new method applied to the quadrilateral membrane element with vertex rigid rotational freedom", *Math. Probl. Eng.*, **2016**(3), 1-13. https://doi.org/10.1155/2016/1045438.

Gutierrez, R.M., Reddy, J.N. and Amabili, M. (2016), "A new twelve-parameter spectral/hp shell finite element for large deformation analysis of composite shells", *Compos. Struct.*, **151**, 183-196. https://doi.org/10.1016/j.compstruct.2016.02.068.

Izzuddin, B.A. (2005), "An enhanced co-rotational approach for large displacement analysis of plates", *Int. J. Numer. Method. Eng.*, **64**(10), 1350-1374. https://doi.org/10.1002/nme.1415.

Izzuddin, B.A. and Liang, Y. (2016), "Bisector and zero-macrospin co-rotational systems for shell elements", *Int. J. Numer. Method. Eng.*, **105**(4), 286-320. https://doi.org/10.1002/nme.4978.

Jeyachandrabose, C., Kirkhope, J. and Babu, C.R. (1985), "An alternative explicit formulation for the DKT plate-bending element", *Int. J. Numer. Method. Eng.*, **21**(7), 1289-1293. https://doi.org/10.1002/nme.1620210709.

Kan, Z., Dong, K., Chen, B., Peng, H. and Song, X. (2021), "The direct force correction based framework for general co-rotational analysis", *Comput. Method. Appl. Mech. Eng.*, **385**, 114018. https://doi.org/10.1016/j.cma.2021.114018.

Katili, I. (1993), "A new discrete Kirchhoff-Mindlin element based on Mindlin-Reissner plate theory and assumed shear strain fields - part II: An extended DKQ element for thick-plate bending analysis", *Int. J. Numer. Method. Eng.*, **36**(11), 1885-1908. https://doi.org/10.1002/nme.1620361107.

Katili, I., Batoz, J.L., Maknun, I.J., Hamdouni, A. and Millet, O. (2015a), "The development of DKMQ plate bending element for thick to thin shell analysis based on the Naghdi/Reissner/Mindlin shell theory", *Finite Elem. Anal. Des.*, **100**, 12-27. https://doi.org/10.1016/j.finel.2015.02.005.

Katili, I., Maknun, I.J., Hamdouni, A. and Millet, O. (2015b), "Application of DKMQ element for composite plate bending structures", *Compos. Struct.*, **132**, 166-174. https://doi.org/10.1016/j.compstruct.2015.04.051.

Kim, K.D., Han, S.C. and Suthasupradit, S. (2007), "Geometrically non-linear analysis of laminated composite structures using a 4-node co-rotational shell element with enhanced strains", *Int. J. Non-Linear Mech.* **42**(6), 864-881. https://doi.org/10.1016/j.ijnonlinmec.2007.03.011.

Ko, Y., Lee, P.S. and Bathe, K.J. (2017a), "A new MITC4+ shell element", *Comput. Struct.*, **182**, 404-418. https://doi.org/10.1016/j.compstruc.2016.11.004.

Ko, Y., Lee, P.S. and Bathe, K.J. (2017b), "The MITC4+shell element in geometric nonlinear analysis", *Comput. Struct.*, **185**, 1-14. https://doi.org/10.1016/j.compstruc.2017.01.015.

Lee, Y., Lee, P.S. and Bathe, K.J. (2014), "The MITC3+ shell element and its performance", *Comput. Struct.*, **138**, 12-23. https://doi.org/10.1016/j.compstruc.2014.02.005.

Li, M. and Zhan, F. (2000), "The finite deformation theory for beam, plate and shell. Part IV. The Fe formulation of Mindlin plate and shell based on Green-Lagrangian strain", *Comput. Method. Appl. Mech. Eng.*, **182**(1-2), 187-203. https://doi.org/10.1016/s0045-7825(99)00092-4.

Long, Y., Cen, S. and Long, Z. (2009), *Advanced Finite Element Method in Structural Engineering*, Tsinghua University Press, Springer Berlin, Heidelberg.

Long, Y.Q. and Xin, K.G. (1989), "Generalized conforming element for bending and buckling analysis of plates", *Finite Elem. Anal. Des.*, **5**(1), 15-30. https://doi.org/10.1016/0168-874x(89)90003-6.

Long, Y. and Xu, Y. (1994a), "Generalized conforming quadrilateral membrane element with vertex rigid rotational freedom", *Comput. Struct.*, **52**(4), 749-755. https://doi.org/10.1016/0045-7949(94)90356-5.

Long, Y. and Xu, Y. (1994b), "Generalized conforming flat

rectangular thin shell element", *Chin. J. Comput. Mech. Appl.* **11**(2), 154-160.

Lu, X., Tian, Y., Cen, S., Guan, H., Xie, L. and Wang, L. (2017), "A high-performance quadrilateral flat shell element for seismic collapse simulation of tall buildings and its implementation in OpenSees", *J. Earthq. Eng.*, **22**(9), 1662-1682. https://doi.org/10.1080/13632469.2017.1297269.

Macneal, R.H. and Harder, R.L. (1985), "A proposed standard set of problems to test finite element accuracy", *Finite Elem. Anal. Des.*, **1**(1), 3-20. https://doi.org/10.1016/0168-874x(85)90003-4.

Meek, J.L. and Ristic, S. (1997), "Large displacement analysis of thin plates and shells using a flat facet finite element formulation", *Comput. Method. Appl. Mech. Eng.*, **145**(3-4), 285-299. https://doi.org/10.1016/s0045-7825(96)01220-0.

Mindlin, R.D. (1951), "Influence of Rotatory inertia and shear on flexural motions of isotropic, elastic plates", *J. Appl. Mech.*, **18**(1), 31-38. https://doi.org/10.1115/1.4010217.

Moita, J.S., Araújo, A.L., Mota Soares, C.M., Mota Soares, C.A. and Herskovits, J. (2016), "Material and geometric nonlinear analysis of functionally graded plate-shell type structures", *Appl. Compos. Mater.*, **23**(4), 537-554. https://doi.org/10.1007/s10443-016-9473-8.

Mororó, L.A.T., Melo, A.M.C., de Parente Junior, E., Lucena Neto, E. and Monteiro, F.A.C. (2020), "Corotational elements for thin-walled laminated composite beams with large 3D rotations", *Thin Wall. Struct.*, **152**, 106375. https://doi.org/10.1016/j.tws.2019.106375.

Nour-Omid, B. and Rankin, C.C. (1991), "Finite rotation analysis and consistent linearization using projectors", *Comput. Method. Appl. Mech. Eng.*, **93**(3), 353-384. https://doi.org/10.1016/0045-7825(91)90248-5.

Nwuzor, I.C., Atuanya, C.U. and Olisa, O. (2021), "Momordica angustisepala fibres and ant hill particles/polyester value-added hybrid composites for bumper application", *World J. Eng.*, **18**(1), 136-145. https://doi.org/10.1108/WJE-03-2020-0096.

Pacoste, C. (1998), "Co-rotational flat facet triangular elements for shell instability analyses", *Comput. Method. Appl. Mech. Eng.* **156**(1-4), 75-110. https://doi.org/10.1016/s0045-7825(98)80004-2.

Rankin, C.C. and Brogan, F.A. (1986), "An element independent corotational procedure for the treatment of large rotations", *J. Press. Vessel Technol. Trans. ASME*, **108**(2), 165-174. https://doi.org/10.1115/1.3264765.

Rankin, C.C. and Nouromid, B. (1988), "The use of projectors to improve finite-element performance", *Comput. Struct.*, **30**(1-2), 257-267. https://doi.org/10.1016/0045-7949(88)90231-3.

Razzaque, A. (1973), "Program for triangular bending elements with derivative smoothing", *Int. J. Numer. Method. Eng.*, **6**(3), 333-343. https://doi.org/10.1002/nme.1620060305.

Reissner, E. (1945), "The effect of transverse shear deformation on the bending of elastic plates", *J. Appl. Mech.*, **12**(2), 69-77. https://doi.org/10.1115/1.4009435.

Sadeghi, K. and Nouban, F. (2019), "An algorithm for simulation of cyclic eccentrically-loaded RC columns using fixed rectangular finite elements discretization", *Comput. Concrete*, **23**(1), 25-36. https://doi.org/10.12989/cac.2019.23.1.025.

Schulz, M. and Filippou, F.C. (2001), "Non-linear spatial Timoshenko beam element with curvature interpolation", *Int. J. Numer. Method. Eng.*, **50**(4), 761-785. https://doi.org/10.1002/1097-0207(20010210)50:4%3C761::AID-NME50%3E3.0.CO;2-2.

Soeb, M.R., Islam, A.B.M.S., Jumaat, M.Z., Huda, N. and Arzu, F. (2017), "Response of nonlinear offshore spar platform under wave and current", *Ocean Eng.*, **144**, 296-304. https://doi.org/10.1016/j.oceaneng.2017.07.042.

Srinivas, S. and Rao, A.K. (1973), "Flexure of thick rectangular plates", *J. Appl. Mech.*, **40**(1), 298-299. https://doi.org/10.1115/1.3422947.

Sze, K.Y., Liu, X.H. and Lo, S.H. (2004), "Popular benchmark problems for geometric nonlinear analysis of shells", *Finite Elem. Anal. Des.*, **40**(11), 1551-1569. https://doi.org/10.1016/j.finel.2003.11.001.

Träff, E.A., Sigmund, O. and Aage, N. (2021), "Topology optimization of ultra high resolution shell structures", *Thin Wall. Struct.*, **160**, 107349. https://doi.org/10.1016/j.tws.2020.107349.

Wang, L., Cen, S., Xie, L. and Lu, X. (2016), "Development of a shear wall model based on a new flat shell element for large deformation simulation and application in opensees", *Eng. Mech.*, **33**(3), 47-54. https://doi.org/10.6052/j.issn.1000-4750.2015.03.0173.

Wang, L., Long, Y. and Long, Z. (2010), "Quadrilateral thin plate elements formulated by the area coordinate method and the shape function spectrum method", *Eng. Mech.*, **27**(8), 1-6.

Wong, F.T., Richard, A. and Katili, I. (2017). "Development of the DKMQ element for buckling analysis of shear-deformable plate bending", *Procedia Eng.*, **171**, 805-812. https://doi.org/10.1016/j.proeng.2017.01.368.

Xu, Y. and Long, Y. (1993). "Quadrilateral membrane element with vertex rotational freedom from generalized compatible condition", *Eng. Mech.*, **10**(3), 27-36.

Yoon, K. and Lee, P.S. (2014). "Nonlinear performance of continuum mechanics based beam elements focusing on large twisting behaviors", *Comput. Method. Appl. Mech. Eng.*, **281**, 106-130. https://doi.org/10.1016/j.cma.2014.07.023.

Zhang, Y.X., Bradford, M.A. and Gilbert, R.I. (2007). "A layered shear-flexural plate/shell element using Timoshenko beam functions for nonlinear analysis of reinforced concrete plates", *Finite Elem. Anal. Des.*, **43**(11-12), 888-900. https://doi.org/10.1016/j.finel.2007.05.002.

*CC*